RESEARCH ARTICLE

An accurate, precise, and affordable light emitting diode spectrophotometer for drinking water and other testing with limited resources

Michael W. Prairie[1], Seth H. Frisbie[2]*, K. Kesava Rao[3], Anyamanee H. Saksri[2], Shreyas Parbat[3], Erika J. Mitchell[4]

1 Department of Electrical and Computer Engineering, Norwich University, Northfield, VT, United States of America, **2** Department of Chemistry and Biochemistry, Norwich University, Northfield, VT, United States of America, **3** Department of Chemical Engineering, Indian Institute of Science, Bangalore, Karnataka, India, **4** Better Life Laboratories, Incorporated, East Calais, VT, United States of America

* sfrisbie@norwich.edu

Abstract

Spectrophotometers are commonly used to measure the concentrations of a wide variety of analytes in drinking water and other matrixes; however, many laboratories with limited resources cannot afford to buy these very useful instruments. To meet this need, an accurate, precise, and affordable light emitting diode (LED) spectrophotometer was designed and built using best engineering practices and modern circuit design. The cost and performance of this LED spectrophotometer was compared against 4 common commercial spectrophotometers. More specifically, the performance of these spectrophotometers was evaluated from the upper limits of linear range, upper limits of operational range, calibration sensitivities, R^2 values, precisions of standards, estimated limits of detection, and percent calibration check standard recoveries for the determinations of iron (Fe), manganese (Mn), and fluoride (F^-) in drinking water. This evaluation was done in the United States (U.S.) and India. Our LED spectrophotometer costs $63 United States Dollars (USD) for parts. The 4 commercial spectrophotometers ranged in cost from $2,424 to $7,644 USD. There are no practical differences in the upper limits of linear range, upper limits of operational range, R^2 values, precisions of standards, and estimated limits of detection for our LED spectrophotometer and the 4 commercial spectrophotometers. For 2 of the 3 analytes, there is a practical difference in the calibration sensitivities our LED spectrophotometer and the 4 commercial spectrophotometers. More specifically, the calibration sensitivities for Mn and F^- using our LED spectrophotometer were 65.2% and 67.0% of those using the 4 commercial spectrophotometers, respectively. In conclusion, this paper describes the design, use, and performance of an accurate, precise, and extremely affordable LED spectrophotometer for drinking water and other testing with limited resources.

Introduction

Spectrophotometers are highly versatile. They are used to measure the concentrations of a wide range of inorganic, organic, and biological chemicals. For example, they are used to measure the concentrations of harmful metals in drinking water [1, 2], active ingredients in pharmaceutical products [3], and clinically important molecules in humans [4]. Commercial spectrophotometers typically cost over $2,000 United States Dollars (USD), a sum which can make these instruments unattainable for organizations with limited resources. In this project, we describe the development of a spectrophotometer which can be built by laboratory technicians or others competent in basic electronics for $63 USD in parts. This spectrophotometer has performance characteristics comparable to 4 commonly used commercial spectrophotometers.

We have observed a definite need for accurate, precise, and affordable spectrophotometers for drinking water and other testing in countries with limited resources. For example, in 1997 an author of this paper helped make the first national-scale map of arsenic (As) affected drinking water in Bangladesh with a 10-to-15-year-old Hach DR/3-analog spectrophotometer [1, 2]. This map suggested that 45 percent (%) of Bangladesh's area has drinking well water with As concentrations greater than the 0.050-milligrams per liter (mg/L) national standard [1, 2]. This important work was done at the International Centre for Diarrhoeal Disease Research, Bangladesh (icddr,b), an international health research organization and the national cholera hospital in Dhaka, Bangladesh. At the time, the analog spectrophotometer was the most expensive instrument in icddr,b laboratory. In contrast, other hospitals and clinics in Dhaka, the nation's capital, did not have any spectrophotometers at all. Also, there were only 6 drinking water testing laboratories in this resource limited country of approximately 120,000,000 people where at least half the water sources have unsafe concentrations of chemicals [1, 2, 5]. We believe that an accurate, precise, and affordable spectrophotometer for drinking water and other testing in regions with limited resources would greatly benefit public health by making it possible to test drinking water sources for metals and other chemicals by using standard spectrophotometric methods.

Commercial spectrophotometers typically use a tungsten filament lamp as a source of visible and near-infrared radiation. This lamp produces a continuum spectrum from about 350 nanometers (nm) to 2,500 nm. A relatively complicated optical system using lenses, slits, and a diffraction grating is often used to filter this polychromatic radiation to nearly monochromatic radiation. This nearly monochromatic radiation is passed through a glass cuvette with a liquid sample or reference solution to a solid-state detector. The amount of radiation absorbed by the liquid sample or reference solution is used to measure the concentration of a specific analyte [6].

This use of nearly monochromatic radiation to measure the concentration of a specific analyte is needed to limit interferences, that is, false positives from other chemicals with similar absorption spectra that might be in the sample matrix. The optical systems of commercial spectrophotometers are relatively expensive and produce nearly monochromatic radiation with spectral bandwidths from about 4 nm to 20 nm [6]. By comparison, light emitting diodes (LEDs) are relatively inexpensive and have similar spectral bandwidths; for example, a large selection of single-color ultraviolet and visible region LEDs are currently available with emission maxima between 250 nm and 680 nm that have spectral bandwidths from 10 nm to 20 nm [7]. Single-color infrared region LEDs are currently available with emission maxima between 750 nm and 1,070 nm that have slightly broader spectral bandwidths from 23 nm to 60 nm [7]. Therefore, the cost of a spectrophotometer could be significantly reduced by replacing the tungsten filament lamp and associated optical system of commercial spectrophotometers with an assortment of carefully selected LEDs; the challenge is then to ensure that the LED spectrophotometer also be highly accurate and precise.

Educators and their students at the high school, college, and university levels often build simple LED spectrophotometers as part of the chemistry, physics, or electronics curriculum [8–16]. These simple LED spectrophotometers are very useful for education; however, they usually have simple power, source, and signal conditioning circuits, which limit their performance. Moreover, they are not rigorously evaluated through comparison with several different commercial instruments, using different analytes and in different regions of calibration curves.

Some commercial LED spectrophotometers are used for specific chemical analyses; for example, Xerox Corporation designed and built a LED spectrophotometer for use in the output paper path of color printers [17]. The designs of these commercial LED spectrophotometers are not freely available. As with other commercial laboratory equipment, the designs are typically patented, requiring contracts and license payments before others can build them with the same design.

Several open source LED spectrophotometers have been developed through robust design processes for potential use in routine laboratories as well as research or teaching [18–24]. These open source spectrophotometers have been reported to have performance capabilities comparable to those of some commercial spectrophotometers. However, these open-source LED spectrophotometers have been designed and tested for just 1 or 2 analytes, and their performance has usually been compared to that of only 1 to 2 commercial spectrophotometers. These projects have generally not examined the upper limits of linear range, upper limits of operational range, calibration sensitivities, and instrument stability in rigorous detail.

In this article, we describe the design, construction, testing, and use of a new accurate, precise, robust, and extremely affordable LED spectrophotometer and make the plans freely available as open source hardware. This LED spectrophotometer was iteratively designed, tested, and improved over a 3-year period by an international team of professors and students of electrical engineering, analytical chemistry, and chemical engineering. This spectrophotometer uses an advanced signal conditioning chain. Another unique feature of this spectrophotometer is that it can be powered by a 6-volt (V) motorcycle battery; this allows the instrument to be used in remote areas. In this paper, we provide a complete list of parts, schematic diagrams of all circuits, and detailed explanations of circuit design and performance testing so that knowledgeable readers can build, test, and use an exact copy of this LED spectrophotometer themselves, making spectrophotometric methods for analyzing drinking water and other key substances such as biological specimens much more affordable for laboratories with limited resources. Readers can build this accurate, precise, robust, and versatile LED spectrophotometer for approximately $63 USD in parts, less than 2.6% of the cost of several commercial spectrophotometers.

Our diverse international team rigorously evaluated this spectrophotometer by comparing its performance with that of 4 different commercial instruments, for 3 different analytes, and in different regions of the calibration curves. Additional novel aspects of this study are the use of higher order polynomial relationships to objectively test the linearity of calibration curves [25] and the use of control charts to estimate detection limits [26]. This new LED spectrophotometer shows performance characteristics comparable to those of 4 commercial spectrophotometers for testing Fe, Mn, and F^- within ranges commonly found in drinking water.

Materials and methods

The requirements, specifications, and component selection choices are summarized in Fig 1. The details of the operation of the various parts are included in the system description, so only summary decisions are included here. Unless otherwise stated, all passive components were easily available resistors with at most 5% tolerance, and capacitors with at most 20% tolerance.

This LED spectrophotometer has 4 subsystems: (1) a power circuit, (2) a LED source circuit, (3) a sample holder, and (4) a photodiode (PD) detector circuit (Figs 2 and 3). A list of the parts and associated prices for building this LED spectrophotometer are shown in Table 1.

The goal of this project was to build a robust spectrophotometer whose performance would be comparable to commercial spectrophotometers while keeping the cost as low as possible. Model numbers of components, suppliers, and costs are presented here to show how much money we paid for these components, but actual costs may vary according to suppliers. Unfortunately, as pointed out by an anonymous reviewer, some components may cost more in resource-limited countries due to limited availability.

Power circuit

The LED spectrophotometer requires a 6-volt (V) minimum to 12-V maximum direct current (DC) input to the power circuit. If there is no municipal power, this 6-V minimum allows the
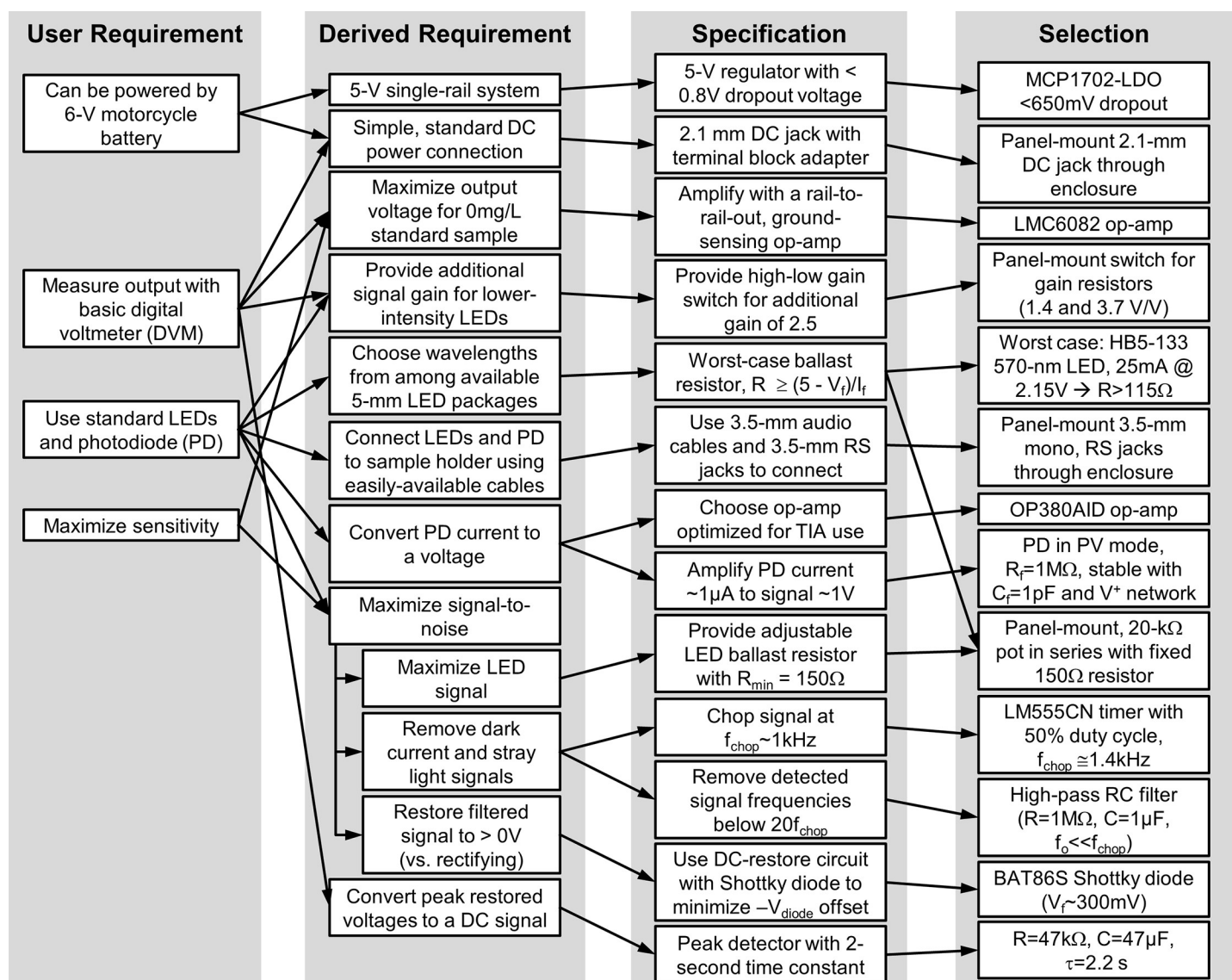
User Requirement	Derived Requirement	Specification	Selection
Can be powered by 6-V motorcycle battery	5-V single-rail system	5-V regulator with < 0.8V dropout voltage	MCP1702-LDO <650mV dropout
	Simple, standard DC power connection	2.1 mm DC jack with terminal block adapter	Panel-mount 2.1-mm DC jack through enclosure
	Maximize output voltage for 0mg/L standard sample	Amplify with a rail-to-rail-out, ground-sensing op-amp	LMC6082 op-amp
Measure output with basic digital voltmeter (DVM)	Provide additional signal gain for lower-intensity LEDs	Provide high-low gain switch for additional gain of 2.5	Panel-mount switch for gain resistors (1.4 and 3.7 V/V)
	Choose wavelengths from among available 5-mm LED packages	Worst-case ballast resistor, $R \geq (5 - V_f)/I_f$	Worst case: HB5-133 570-nm LED, 25mA @ 2.15V → R>115Ω
Use standard LEDs and photodiode (PD)	Connect LEDs and PD to sample holder using easily-available cables	Use 3.5-mm audio cables and 3.5-mm RS jacks to connect	Panel-mount 3.5-mm mono, RS jacks through enclosure
	Convert PD current to a voltage	Choose op-amp optimized for TIA use	OP380AID op-amp
Maximize sensitivity		Amplify PD current ~1µA to signal ~1V	PD in PV mode, R_f=1MΩ, stable with C_f=1pF and V⁺ network
	Maximize signal-to-noise		
	Maximize LED signal	Provide adjustable LED ballast resistor with R_{min} = 150Ω	Panel-mount, 20-kΩ pot in series with fixed 150Ω resistor
	Remove dark current and stray light signals	Chop signal at f_{chop}~1kHz	LM555CN timer with 50% duty cycle, $f_{chop} \cong 1.4$kHz
		Remove detected signal frequencies below 20f_{chop}	High-pass RC filter (R=1MΩ, C=1µF, $f_o << f_{chop}$)
	Restore filtered signal to > 0V (vs. rectifying)	Use DC-restore circuit with Shottky diode to minimize –V_{diode} offset	BAT86S Shottky diode (V_f~300mV)
	Convert peak restored voltages to a DC signal	Peak detector with 2-second time constant	R=47kΩ, C=47µF, τ=2.2 s

Fig 1. The requirements, specifications, and component selection of the light emitting diode (LED) spectrophotometer.
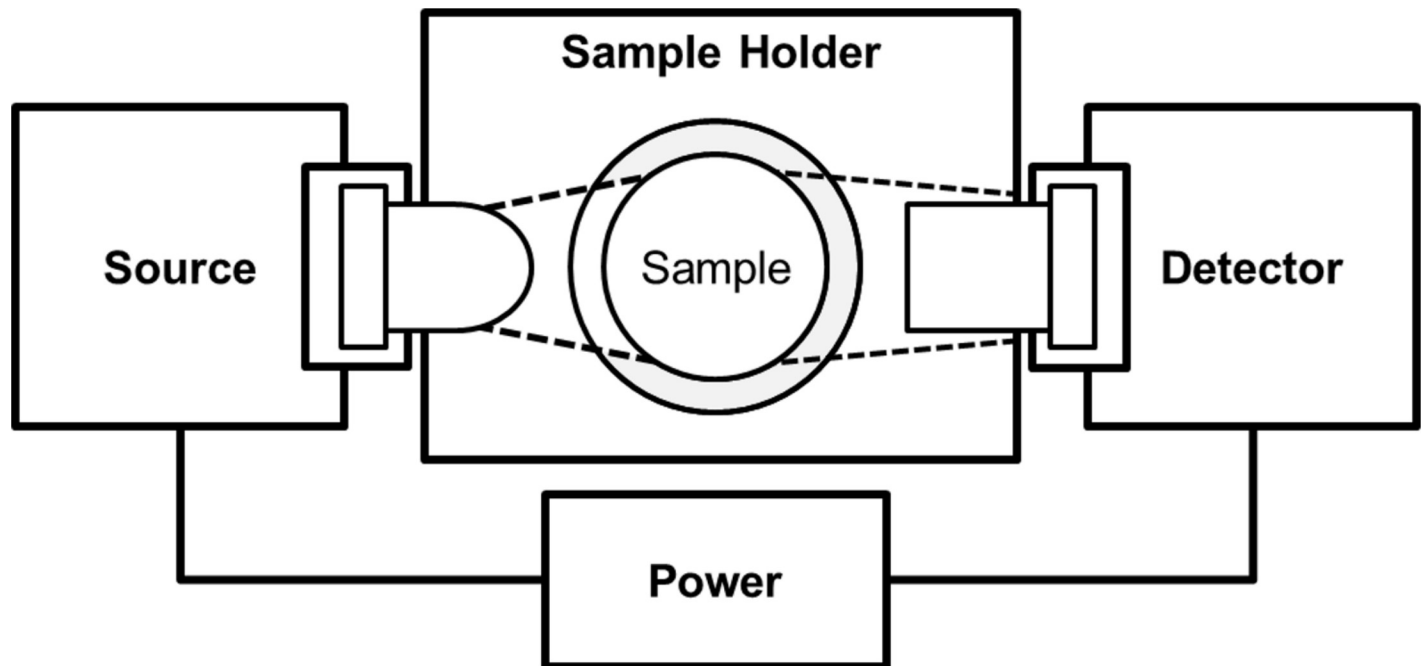
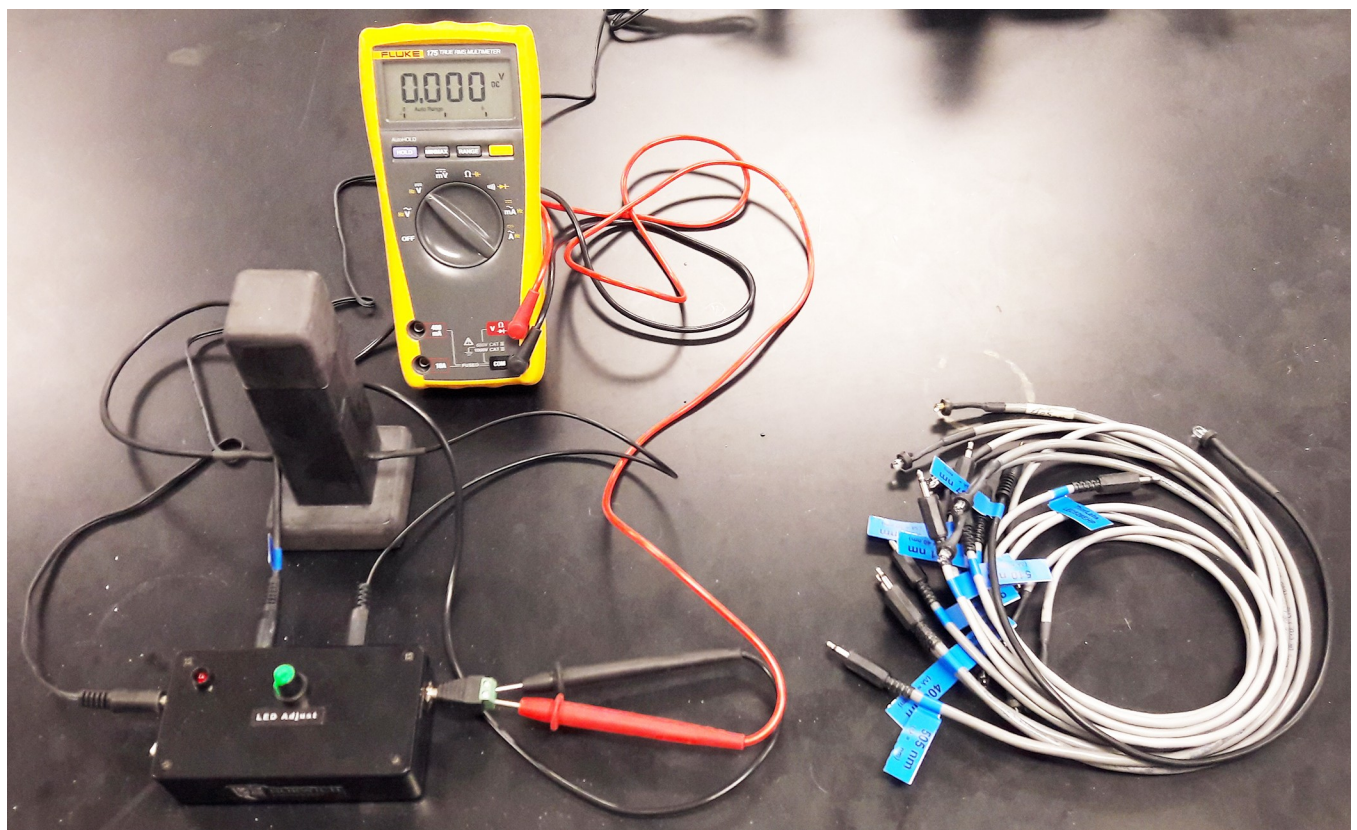**Fig 2. A block diagram of the light emitting diode (LED) spectrophotometer.**

Fig 3. A photograph of the light emitting diode (LED) spectrophotometer.

Table 1. A list of the parts and associated prices in current (2019) United States Dollars (USD) for 1 light emitting diode (LED) spectrophotometer. These prices are from Newark (www.newark.com), Digi-Key Electronics (www.digikey.com), and Amazon.com, Inc. (www.amazon.com).

Part	Value	Device	Package	Description	Price
C1	1 picofarad (pF)	561R10TCCV10	Radial, 6.4-millimeter (mm) pitch	Capacitor	0.79
C2	1 microfarad (µF)	MCCB1E105M2ACB	Radial, 5.08 mm pitch	Capacitor	0.58
C3	0.1 µF	MCDTR10M35-1-RH	Radial, 2.5 mm pitch	Capacitor	0.75
C4	0.01 µF	562R5GAS10	Radial, 6.4 mm pitch	Capacitor	0.65
C5	33 pF	561R10TCCQ33	Radial, 6.4 mm pitch	Capacitor	1.07
C6	47 µF	ECA-1HM470	Radial, 2.5 mm pitch	Polarized capacitor	0.25
C7	10 µF	EEA-FC1E100	Radial, 1.5 mm pitch	Polarized capacitor	0.30
C9	1 µF	MCCB1E105M2ACB	Radial, 5.08 mm pitch	Capacitor	0.58
C14	0.1 µF	MCDTR10M35-1-RH	Radial, 2.5 mm pitch	Capacitor	0.75
C15	0.1 µF	MCDTR10M35-1-RH	Radial, 2.5 mm pitch	Capacitor	0.75
C16	0.1 µF	MCDTR10M35-1-RH	Radial, 2.5 mm pitch	Capacitor	0.75
C18	0.1 µF	MCDTR10M35-1-RH	Radial, 2.5 mm pitch	Capacitor	0.75
C19	0.1 µF	MCDTR10M35-1-RH	Radial, 2.5 mm pitch	Capacitor	0.75
D1		BAT86	DO-34 (SOD68)	Schottky diode	0.39
D2		BAT86	DO-34 (SOD68)	Schottky diode	0.39
IC1		OPA380AID	8-SOIC	Transimpedance amplifier	5.46
IC2		LMC6082IN/NOPB	8-DIP	Operational amplifier	4.69
IC3		LM1117T-5.0/NOPB	TO-220	Voltage regulator	1.54
IC4		LMC555CN/NOPB	8-DIP	CMOS timer	1.35
LED		Green LED—520 nanometer (nm)	T-1 ¾	520 nm (one of several wavelengths)	0.32
LED_ON		SSL-LX5093LID	T-1 ¾	LED	0.45
ON/OFF		RA11131100	Panel mount	SPST rocker switch	0.49
GAIN_SW		1MS1T1B5M1QE	Panel mount	SPDT toggle switch	1.40
PD		PDB-C139	Radial, 5 mm diameter (T 1 3/4)	Photodiode	4.82
Q1		2N7000	TO-92	N-Channel MOSFET	0.43
R1	1 megaohm (MΩ)	MCF 0.25W 1M	Axial leaded	Resistor	0.09
R2	1 MΩ	MCF 0.25W 1M	Axial leaded	Resistor	0.09
R3	1 MΩ	MCF 0.25W 1M	Axial leaded	Resistor	0.09
R4	47 kilo-ohm (kΩ)	MCF 0.25W 47K	Axial leaded	Resistor	0.09
R5	5.6 kΩ	MCF 0.25W 5K6	Axial leaded	Resistor	0.09
R6	2.2 kΩ	MCF 0.25W 2K2	Axial leaded	Resistor	0.09
R7	5.1 kΩ	MCCFR0W4J0512A50	Axial leaded	Resistor	0.01
R8	150 Ω	MCCFR0W4J0151A50	Axial leaded	Resistor	0.01
R9	1 kΩ	MCF 0.25W 1K	Axial leaded	Resistor	0.09
R10	20 kΩ POT	P160KN-0QC15B20K	Panel mount	Potentiometer	0.79
R11	15 kΩ	MCCFR0W4J0153A50	Axial leaded	Resistor	0.07
		Various vendors	8-DIP	8-SOIC to 8-DIP adapter	< 1.00
		MC002825	Panel mount	2.1 mm DC power jack	0.58
		MC002825	Panel mount	2.1 mm DC power jack	0.58
		MJ-074N	Panel mount	3.5 mm Audio jack	1.54
		MJ-074N	Panel mount	3.5 mm Audio jack	1.54
		PSG03744	Cable	3.5 mm Stereo male-male cable (cut in half)	0.57
		CLB-JL-8111	Accessory	2.1 mm plug to terminal adapter	2.00
		PPW00026	Accessory / cable	Male DC 2.1 mm pigtail	1.15
		28–965	Enclosure	Plastic project box	4.04
		MRG1791.0050	Cable	RG-178U coax (12 inches; for PD cable)	.40

(Continued)

Table 1. (Continued)

Part	Value	Device	Package	Description	Price
		38K6105	Jack assembly	3.5 mm Mono male jack (for PD cable)	0.93
		MC72601S	Knob for 6 mm shaft	Rotatory potentiometer knob	0.75
		A104800AAC	Panel mount	5 mm LED holder	1.80
		503	Copper clad FR4	Single-sided printed circuit board	4.65
		437	Moldable silicone rubber	Sugru moldable glue	2.28
		F-3599	9.525 mm Square	Bumper / feet, stick on (8)	4.66
		09300	Machine screw, 4–40, 6.35 mm	PCB mounting hardware (4)	0.40
		SK00-0044-AKS	Screw nuts, 4–40	PCB mounting hardware (4)	0.32
		DM3-FASTWAZ100DIN125	Washer, 3 mm ID	PCB mounting hardware (8)	0.07
		24–14687	22 AWG stranded wire	PCB to panel component (estimated cost)	0.50
		HS511-1.22M	3 mm	Heat shrink tubing (estimated cost)	0.10
			0.75 x 1.5 x 12 inch 0.75 x 3.5 x 3.5 inch	Wood material for sample holder (estimated cost)	1.10
		75H5807	Nylon cable clamp, 0.5 inch	Sample holder spring	0.08
				Total cost	63.00

LED spectrophotometer to run off a 6-V motorcycle battery. The power circuit provides a stable and constant 5-V regulated DC output to the LED source and PD detector circuits regardless of the 6-V to 12-V input voltage (Fig 4). The design requirement to run off a 6-V motorcycle battery called for a low-dropout (LDO) linear regulator to accommodate the 1-V difference between the 6-V minimum input and 5-V regulated output voltages. A standard linear regulator typically requires a 2-V difference between the minimum input and regulated output voltages [27, 28]. A LM1117-LDO regulator was selected to match these design requirements for the power circuit (Table 1; Fig 4). This regulator has an input voltage that ranges from a 5.35-V minimum to a 13.2-V maximum, a dropout voltage of 650 millivolt (mV), and a maximum current rating of 250 milliamperes (mA).

The power circuit has a manual on-off switch (Table 1; Fig 4). If the power circuit is on, an indicator LED is automatically illuminated (Table 1; Fig 4). The capacitors reduce noise by shunting high-frequency noise from the positive terminal to the ground terminal (Table 1; Fig 4). The 1-kilo-ohm (kΩ) ballast resistor limits the current to the indicator LED (Table 1; Fig 4). The forward voltage of the indicator LED is approximately 2 V; therefore, the 1-kΩ ballast resistor limits the current to approximately 3 mA (Fig 4).
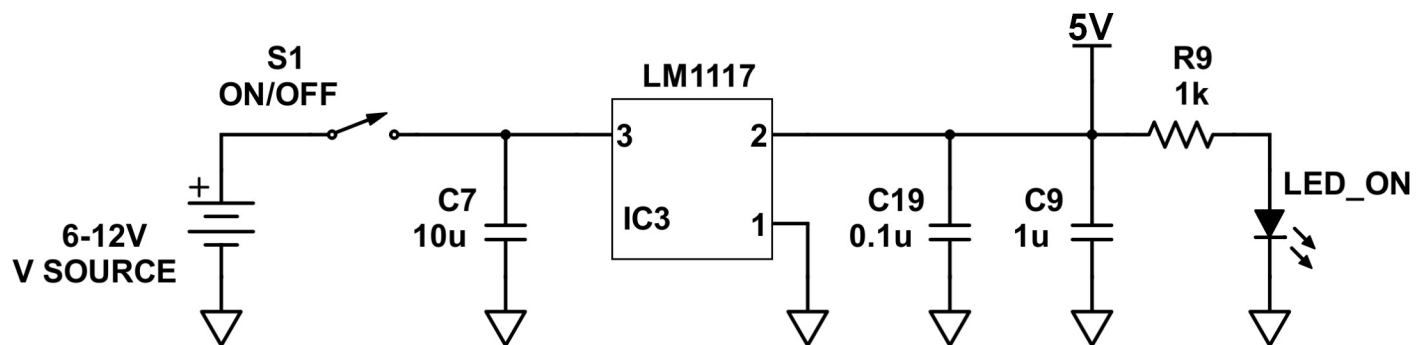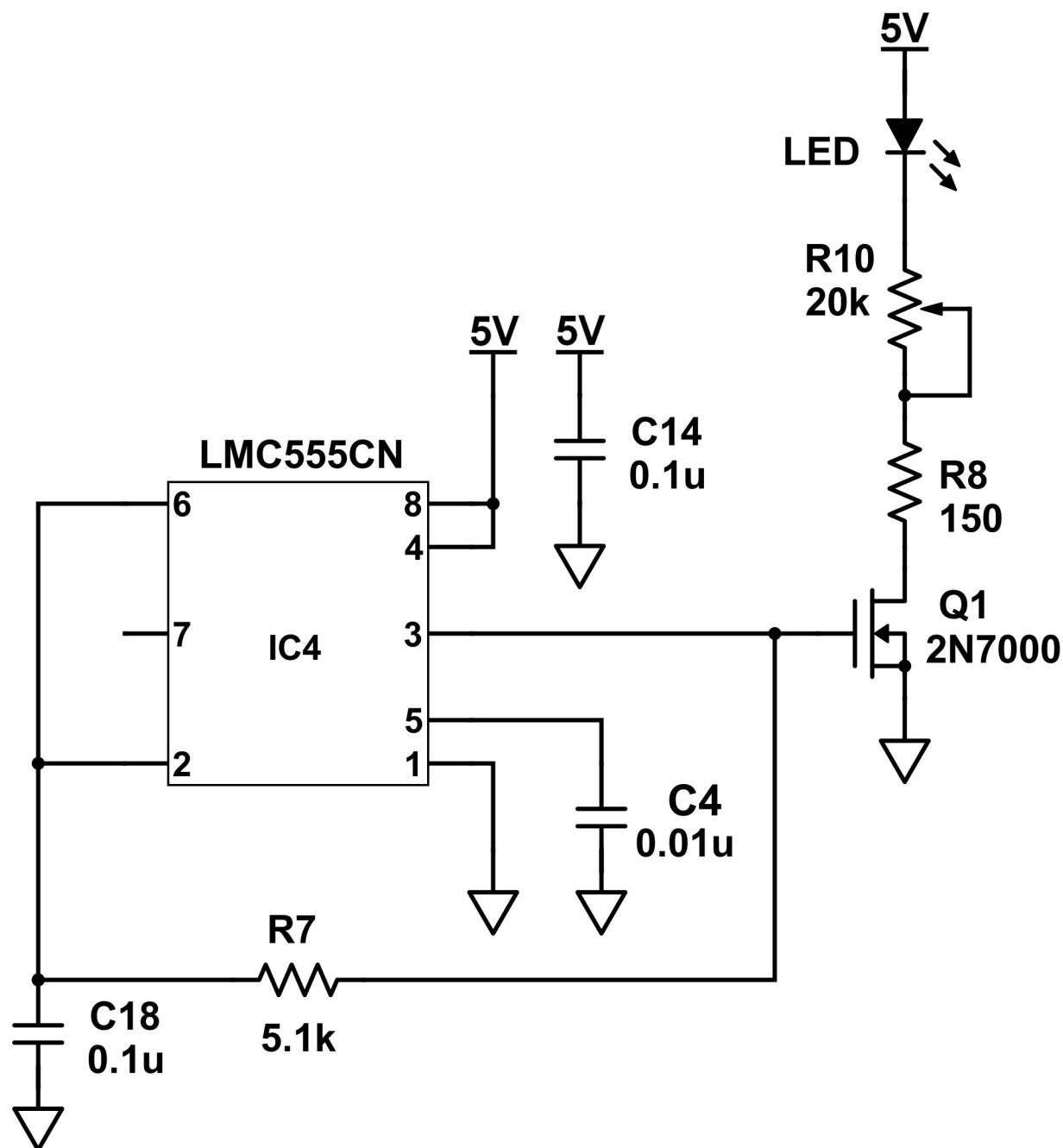

Fig 4. A schematic diagram of the power circuit.

Fig 5. A schematic diagram of the light emitting diode (LED) source circuit.

Light emitting diode source circuit

The source LED is powered by the 5-V regulated DC output of the power circuit. The source LED is controlled by a driver circuit that uses a LM555CN timer circuit (integrated circuit) and a 2N7000-metal-oxide-semiconductor field-effect transistor (MOSFET; Table 1; Fig 5) [28].

The timer circuit is used to generate a square wave of voltage to the transistor (Fig 5). More specifically, the LM555CN timer circuit provides a 50% duty cycle (the voltage to the transistor

is 50% on and then 50% off during each cycle) at a 1.4-kilohertz (kHz) frequency [28]. This duty cycle and chopping frequency are determined by the 5.1-kΩ resistor (R7) and 0.1-microfarad (μF) capacitor (C18; Table 1; Fig 5) [28]. Capacitor C4 is a 0.01-μF bypass capacitor at the control voltage pin (5) of the timer circuit (Table 1; Fig 5). Capacitor C14 is a 0.1-μF bypass capacitor at the connection to the power circuit (Table 1; Fig 5).

The 2N7000-MOSFET transistor is used as a switch to turn the source LED on and off in response to the square wave of voltage from the timer circuit (Fig 5). Therefore, the source LED generates an on-off square wave of emitted light through the sample holder and to the PD detector circuit (Figs 2, 3 and 5). If the source LED is on, the detector signal results from the light that is transmitted through the sample holder, any stray light from the environment, and any dark current from the random generation or recombination of electron-hole pairs in the photodiode [29]. If the source LED is off, the detector signal results from any stray light, and any dark current [29]. Therefore, stray light and dark current produce a constant DC voltage shift during both the on and off portions of the detector signal. The source LED is modulated at 1.4 kHz so that this DC voltage shift can be removed by a high-pass filter in the PD detector circuit.

A fixed 150-ohm (Ω) ballast resistor (R8) limits the maximum forward current to 30 mA and prevents the source LED from burning out (Table 1; Fig 5). This fixed ballast resistor (R8) is connected in series with a potentiometer (R10; Table 1; Fig 5). The potentiometer (R10) has a 20-kΩ maximum resistance and is used to adjust the brightness of the source LED and prevent saturating the PD detector circuit (Table 1; Fig 5). A typical forward voltage is about 3.5 V when the source LED is on.

The source LED was selected so that the wavelength of the emission maximum of the source LED corresponded to the wavelength of the absorption maximum of the colorized analyte. For example, a source LED with an emission maximum at 510 nanometers (nm) was used for the analysis of a colorized analyte with an absorption maximum at 510 nm. The spectral width of this source LED is about 25 nm, according to the manufacturer (Table 1).

Sample holder

The sample holder is shown in Figs 2, 3 and 6. It is made mostly of wood (Fig 3). It holds a standard 1.0-centimeter (cm) diameter silicate glass sample cell (Fig 6). It uses a modified nylon cable clamp as a spring to reproducibly hold the sample cell in the sample holder (Fig 6). A wooden cap prevents stray ambient light from entering the sample holder (Fig 6). Finally, the interior of the sample holder is painted black to absorb stray light (Fig 3).

Photodiode detector circuit

The detector PD is powered by the 5-V regulated DC output of the power circuit. The PD is connected to a signal conditioning chain. This chain uses a transimpedance amplifier, a high-pass filter, a DC-restore circuit, a peak detector, and a final stage amplifier (Fig 7).

The PDB-C139-photodiode is used in photoconductive mode to convert the light that is transmitted through the sample cell to a signal current (PDB-C139; Table 1). The power of this incident light at the PD is directly proportional to the signal current that is output by the PD. This incident power at the PD is roughly 5 microwatts (μW) or less. The responsivity of the PD depends on the wavelength of absorbed light and ranges from approximately 0.15 to 0.25 ampere/Watt (A/W). Therefore, the signal current is roughly 1 microamperes (μA) or less as shown in Eq 1.

$$\lesssim 5 \ \mu W \times \frac{1 \ W}{10^6 \ \mu W} \times \frac{\sim 0.2 \ A}{1 \ W} \times \frac{10^6 \ \mu A}{1 \ A} \lesssim 1 \ \mu A \qquad (1)$$
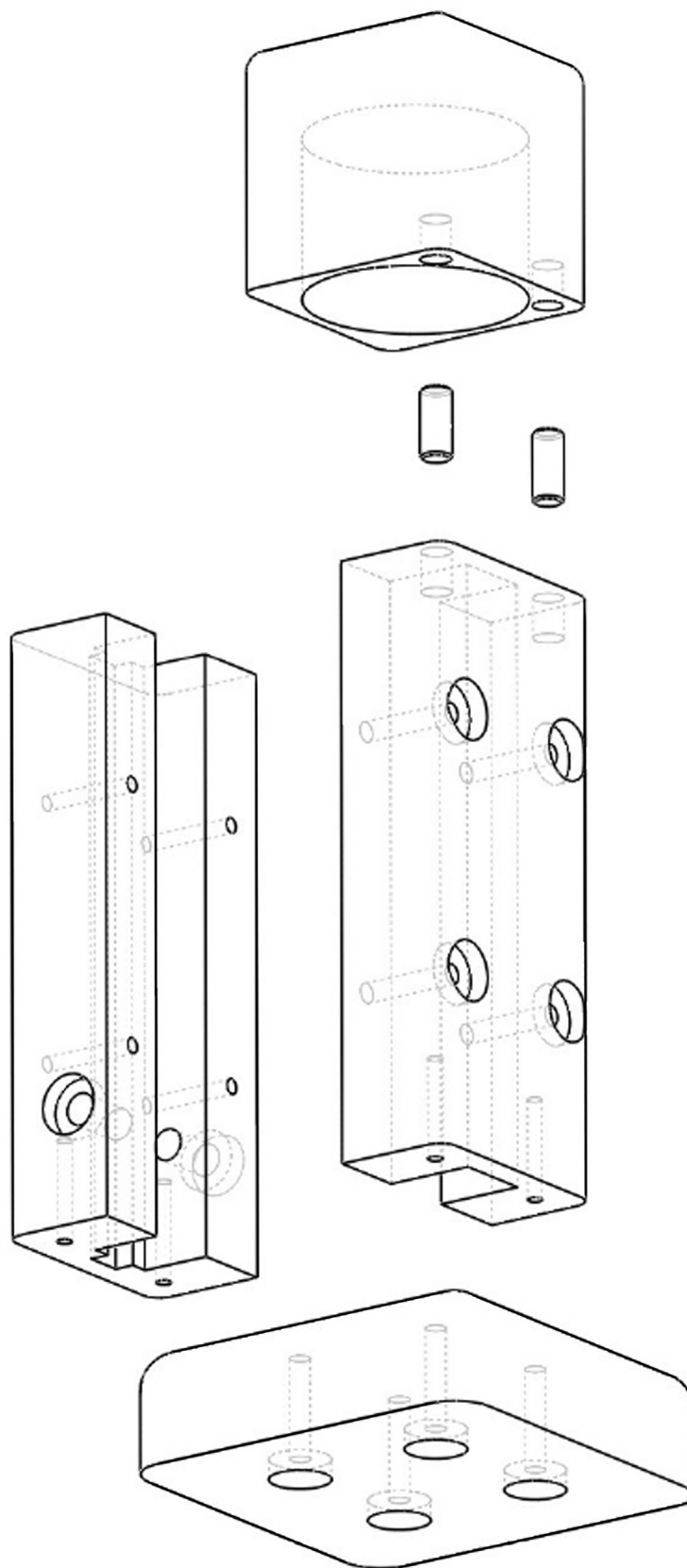
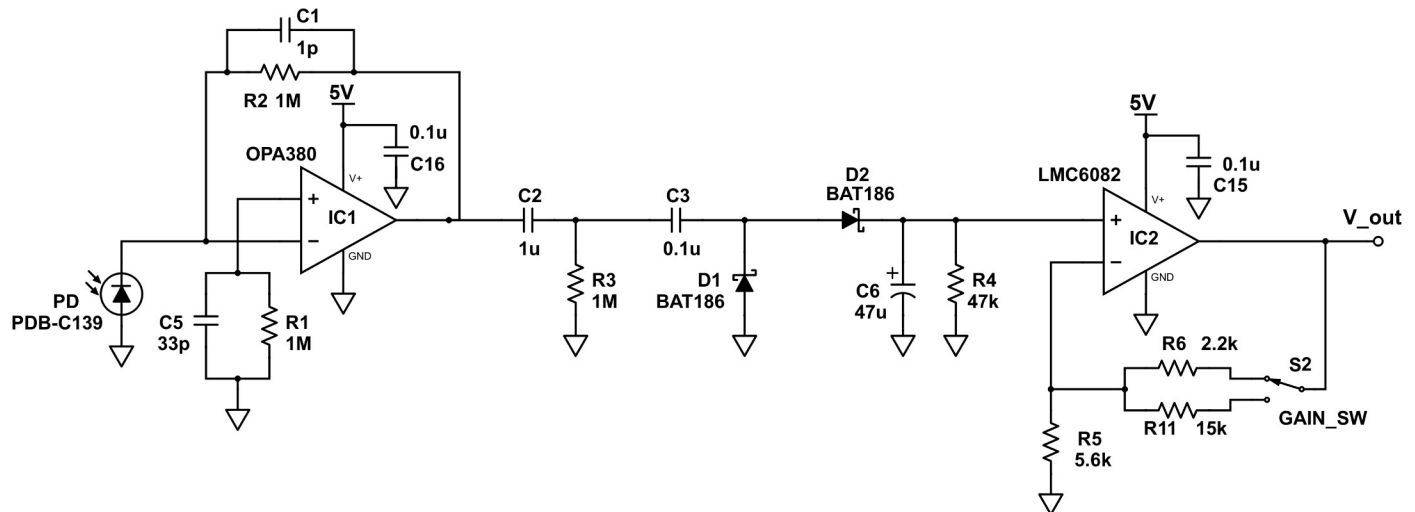**Fig 6. An exploded view of the sample cell holder.**

Fig 7. A schematic diagram of the photodiode (PD) detector circuit. The signal conditioning chain uses a transimpedance amplifier, a high-pass filter, a DC-restore circuit, a peak detector, and a final stage amplifier.

https://doi.org/10.1371/journal.pone.0226761.g007

The OPA380AID operational amplifier is optimized for use as a transimpedance amplifier (TIA; Table 1; Fig 7). The TIA converts the relatively small signal current from the PD to a usable signal voltage. The TIA has relatively small input bias currents, relatively small input offset voltages, and a relatively large gain bandwidth. The gain of the TIA is set by a 1-mega-ohm (MΩ) feedback resistor (R2; Table 1; Fig 7). More specifically, a transimpedance gain of $v_0/i_i = 10^6$ V/A from this 1-MΩ feedback resistor (R2) provides a usable signal voltage that is on the order of 1 V from the relatively small signal current that is on the order of 1 μA as shown in Eq 2.

$$1 \ \mu A \times \frac{1 \ A}{10^6 \ \mu A} \times \frac{10^6 \ V}{1 \ A} = 1 \ V \qquad (2)$$

The 1-picofarad (pF) capacitor (C1) that is in parallel with the 1-MΩ feedback resistor (R2) is used to reduce noise (Table 1; Fig 7). More specifically, this capacitor (C1) compensates for the capacitance of the PD introducing a pole in the feedback path at high frequencies; this prevents oscillation of the signal (Fig 7). Similarly, the 33-pF capacitor (C5) in parallel with the 1-MΩ resistor (R1) is also used to reduce noise (Table 1; Fig 7). More specifically, this capacitor (C5) and resistor (R1) compensate for the small input bias currents and offset voltages by matching the impedance at the positive and negative input terminals of the operational amplifier (Fig 7).

The TIA output signal voltage has a small, positive offset from stray light, and dark current. This offset is removed with a high-pass filter, and a DC-restore circuit. The high-pass filter shifts the average value of the square wave detector signal to 0 V; it uses a 1-microfarad (μF) capacitor (C2) and a 1-MΩ resistor (R3; Table 1; Fig 7). The cutoff frequency (f_{HPF}) of this high-pass filter is 0.16 Hz; that is, this filter passes signals greater than 0.16 Hz, and attenuates signals less than 0.16 Hz (Eq 3).

$$f_{HPF} = \frac{1}{2\pi C_2 R_3} = \frac{1}{\left(2 \times \pi \times 1 \ \mu F \times \frac{1 \ F}{10^6 \ \mu F} \times \frac{\frac{1}{\Omega} s}{1 \ F} \times 1 \ M\Omega \times \frac{10^6 \ \Omega}{1 \ M\Omega} \right)} = 0.16 \ Hz \qquad (3)$$

This DC-restore circuit is a diode clamping circuit; it shifts the minimum value of the square

wave detector signal to 0 V [30]. Therefore, the output of the DC-restore circuit is a square wave of signal voltages that ranges from approximately 0 V to some positive voltage, depending on the concentration of analyte in the sample cell [30]. This DC-restore circuit uses a 0.1-μF capacitor (C3) and a BAT86-Schottky diode (D1; Table 1; Fig 7). When the input signal voltage is negative, the Schottky diode (D1) is forward-biased, the 0.1-μF capacitor (C3) charges, and the output signal voltage is 0 V minus the small forward voltage drop of the Schottky diode (Fig 7) [30]. When the input signal voltage is positive, the Schottky diode (D1) is reverse-biased, the 0.1-μF capacitor (C3) retains its charge, and the output signal voltage equals the input signal voltage plus the capacitor voltage (D1; Fig 7) [30]. Therefore, the dark current and stray light signal are removed, and the full magnitude of the signal voltage is restored [31].

The peak detector circuit uses the Schottky diode (D2), a 47-μF capacitor (C6), and a 47-kΩ resistor (R4; Table 1; Fig 7). The capacitor (C6) is charged by the peak signal voltage (Fig 7). The resistor (R4) allows the capacitor (C6) to discharge with a time constant of 2.2 second (s) as shown in Eq 4 (Fig 7).

$$47 \ \mu F \times \frac{1 \ F}{10^6 \ \mu F} \times \frac{\frac{1 \ s}{\Omega}}{1 \ F} \times 47 \ k\Omega \times \frac{10^3 \ \Omega}{1 \ k\Omega} = 2.2 \ s \tag{4}$$

The final stage amplifier uses a LMC6082-non-inverting operational amplifier with a switchable gain of 1.4 or 3.7 V/V (Table 1; Fig 7). This is a rail-to-rail input, ground-sensing operational amplifier in a single-rail system. The upper rail is the 5-V system voltage, and the lower rail is the 0-V ground reference voltage. This is critical since the peak signal voltage from highly concentrated samples will be close to 0 V; this rail-to-rail input, ground-sensing capability helps minimize error from measuring the small differences in these voltages. The lower 1.4 V/V gain option is used if the maximum intensity of the source LED is sufficient to maximize the TIA output. The higher 3.7-V/V gain option is used if the maximum intensity of the source LED is not sufficient to produce a large TIA output. The final signal voltage is read with a standard voltmeter (Figs 3 and 7).

Calculating price

A list of the parts and associated prices for building one of the 2 identical LED spectrophotometers used in this study are shown in Table 1. The 3 commercial spectrophotometers used for this study in the United States (U.S.), a Hach DR-2700, a Hach 2010, and a Thermal Electron Spectronic 20D+ are no longer manufactured [32, 33]. So that comparisons of prices in current (2019) USD could be made, the historical manufacturer's suggested retail price (MSRP) for each of these instruments was adjusted for inflation with the consumer price index (CPI) inflation calculator [34]. These prices are shown in Tables 2 and 3. In contrast, the 1 commercial ultraviolet-visible (UV-Vis) absorption spectrophotometer used for this study in India, an Agilent Technologies Cary 60-UV-Vis is currently manufactured [35]. The price for this instrument in current (2019) USD is shown in Table 4.

Total iron (Fe) by the 1,10-phenanthroline method

The concentrations of total iron (Fe) were determined by the 1,10-phenanthroline method [36]. The absorbance of the complexed Fe product was measured at 510 nm with a Hach DR-2700, a Hach 2010, a Thermal Electron Spectronic 20D+, and 2 identical LED spectrophotometers (Table 2; Figs 8–10). Standard solutions at 0.00, 1.01, 2.00, 3.00, 3.99, 4.99, 5.99, 6.99, 7.98, 8.98, and 9.98 mg/L of total Fe were used to calculate linear range [25], operational range [36], and calibration sensitivity [6, 38]. Seven 0.00-mg/L standard solutions were analyzed as samples and used to calculate the precision of standards [36], and the estimated limit of

Table 2. The price and performance of a Hach DR-2700, a Hach 2010, a Thermal Electron Spectronic 20D+, and 2 identical light emitting diode (LED) spectrophotometers for the determination of total iron (Fe) by the 1,10-phenanthroline method [36]. V_0 = blank voltage.

Price and Performance	Hach DR-2700	Hach 2010	Spectronic 20D+	LED Spectrophotometer #1				LED Spectrophotometer #2			
				$V_0 = 4.364$	$V_0 = 3.872$	$V_0 = 3.364$	$V_0 = 2.842$	$V_0 = 4.364$	$V_0 = 3.872$	$V_0 = 3.366$	$V_0 = 2.846$
Price in current (2019) United States Dollars (USD)	3,442	2,907	2,424	63	63	63	63	63	63	63	63
Upper limit of linear range (mg/L)	3.00	6.99	3.00	3.00	3.99	3.00	3.00	4.99	3.99	3.00	3.99
Upper limit of operational range (mg/L)	7.98	7.98	7.98	6.99	6.99	6.99	6.99	7.98	7.98	7.98	7.98
Calibration sensitivity (L/mg) using linear regression through the origin for the 0.00, 1.01, 2.00, and 3.00 mg/L standards	0.174	0.180	0.165	0.138	0.136	0.138	0.138	0.163	0.165	0.167	0.169
R^2 for the linear regression through the origin for the 0.00, 1.01, 2.00, and 3.00 mg/L standards	0.99999	1.00000	0.99994	0.99992	0.99998	0.99992	0.99980	0.99999	0.99999	0.99999	0.99997
Precision of standards (mg/L)	0.002	0.003	0.002	0.005	0.004	0.003	0.005	0.007	0.005	0.009	0.009
Estimated limit of detection (mg/L)	0.003	0.004	0.003	0.006	0.005	0.004	0.006	0.008	0.006	0.010	0.010
% Calibration check standard recovery	99.6	99.8	99.6	99.4	99.1	99.2	99.0	100.0	99.3	99.2	98.8

detection [26]. Lastly, a 3.00-mg/L standard solution was analyzed as a sample and used to calculate the % calibration check standard recovery [36]. This work was done at Norwich University in Northfield, Vermont (VT).

Total manganese (Mn) by the 1-(2-pyridylazo)-2-naphthol method

The concentrations of total manganese (Mn) were determined by the 1-(2-pyridylazo)-2-naphthol (PAN) method [37]. The absorbance of the complexed Mn product was measured at 560 nm with a Hach DR-2700, a Hach 2010, a Thermal Electron Spectronic 20D+, and a LED spectrophotometer (Table 3; Figs 11 and 12). Standard solutions at 0.000, 0.100, 0.200, 0.300, 0.400, 0.500, 0.600, 0.700, 0.800, 0.900, and 1.000-mg/L of total Mn were used to calculate linear range [25], operational range [36], and calibration sensitivity [6, 38]. Seven 0.000-mg/L standard solutions were analyzed as samples and used to calculate the precision of standards [36], and the estimated limit of detection [26]. Lastly, a 0.300-mg/L standard solution was analyzed as a sample and used to calculate the % calibration check standard recovery [36]. This work was done at Norwich University in Northfield, VT.

Table 3. The price and performance of a Hach DR-2700, a Hach 2010, a Thermal Electron Spectronic 20D+, and a light emitting diode (LED) spectrophotometer for the determination of total manganese (Mn) by the Hach 1-(2-pyridylazo)-2-naphthol (PAN) method [37]. V_0 = blank voltage.

Price and Performance	Hach DR-2700	Hach 2010	Spectronic 20D+	LED Spectrophotometer #1			
				$V_0 = 1.989$	$V_0 = 1.553$	$V_0 = 1.011$	$V_0 = 0.529$
Price in current (2019) United States Dollars (USD)	3,442	2,907	2,424	63	63	63	63
Upper limit of linear range (mg/L)	0.500	0.600	0.700	0.500	0.600	0.500	0.400
Upper limit of operational range (mg/L)	≥ 1.000	≥ 1.000	≥ 1.000	≥ 1.000	≥ 1.000	≥ 1.000	≥ 1.000
Calibration sensitivity (L/mg) using linear regression through the origin for the 0.000, 0.100, 0.200, and 0.300 mg/L standards	0.798	0.828	0.781	0.558	0.542	0.532	0.463
R^2 for the linear regression through the origin for the 0.000, 0.100, 0.200, and 0.300 mg/L standards	0.99995	0.99997	0.99987	0.99961	0.99943	0.99948	0.99990
Precision of standards (mg/L)	0.0006	0.0006	0.003	0.001	0.005	0.002	0.003
Estimated limit of detection (mg/L)	0.0007	0.0007	0.003	0.001	0.006	0.002	0.004
% Calibration check standard recovery	98.8	99.2	107.7	98.3	99.0	99.2	98.4

Table 4. The price and performance of an Agilent Technologies Cary 60 UV-Vis (ultraviolet-visible) absorption spectrophotometer, and a light emitting diode (LED) spectrophotometer for the determination of total fluoride (F⁻) by the sodium 2-(parasulfophenylazo)-1,8-dihydroxy-3,6-naphthalene disulfonate (SPADNS) method [36]. V_0 = blank voltage.

Price and Performance	Agilent Technologies Cary 60 UV-Vis	LED Spectrophotometer #1					
		$V_0 = 0.627$	$V_0 = 0.550$	$V_0 = 0.525$	$V_0 = 0.486$	$V_0 = 0.407$	$V_0 = 0.358$
Price in current (2019) United States Dollars (USD)	7,644	63	63	63	63	63	63
Upper limit of linear range (mg/L)	1.599	0.000[a]	1.399	1.000	1.399	1.000	1.800
Upper limit of operational range (mg/L)	1.399	1.599	1.399	1.399	1.399	1.399	0.201
Calibration sensitivity (L/mg) using linear regression through the origin for the 0.000, 0.201, 0.400, and 0.601 mg/L standards	0.127	0.107	0.085	0.102	0.087	0.079	0.051
R^2 for the linear regression through the origin for the 0.000, 0.201, 0.400, and 0.601 mg/L standards	0.99494	0.99876	0.99828	0.99904	0.99845	0.99914	0.98948
Precision of standards (mg/L)	0.01	0.005	0.006	0.009	0.01	0.01	0.03
Estimated limit of detection (mg/L)	0.01	0.006	0.008	0.01	0.01	0.02	0.03
% Calibration check standard recovery	96.8	100.9	100.0	101.2	101.5	104.0	103.6

[a]The 4 lowest concentrations of standard (0.000, 0.201, 0.400, and 0.601 mg/L) gave a quadratic effect coefficient that is different from 0 at the 95% confidence level (p-value = 0.0251); therefore, the calibration curve is nonlinear and the upper limit of linear range is 0.000 mg/L.

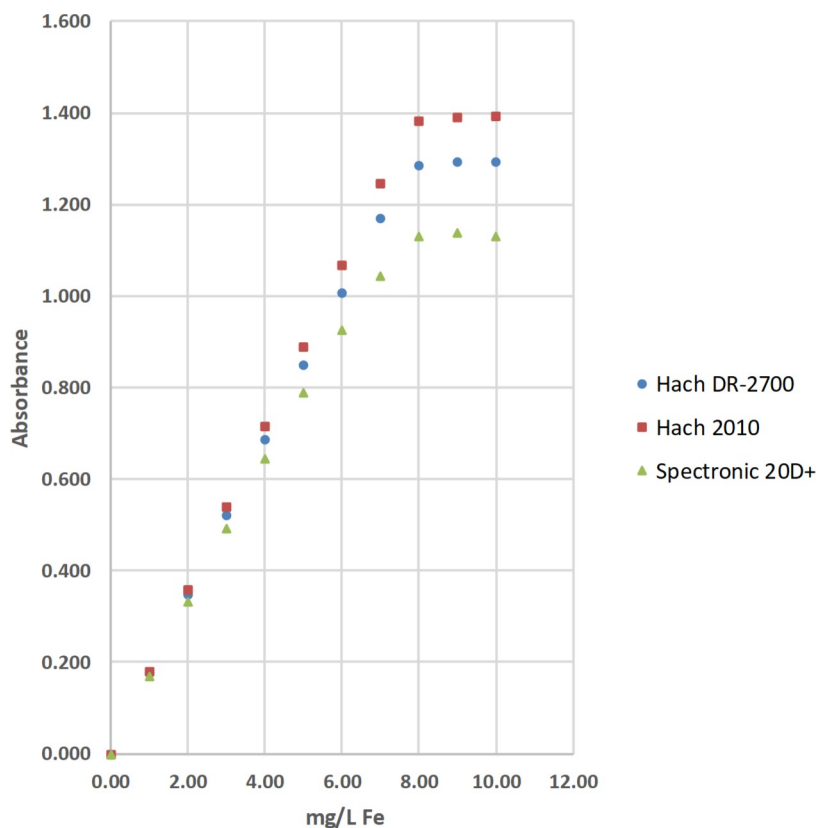https://doi.org/10.1371/journal.pone.0226761.t004

Fig 8. The calibration results for the determination of total iron (Fe) by the 1,10-phenanthroline method using a Hach DR-2700, a Hach 2010, and a Thermal Electron Spectronic 20D+ spectrophotometer [36].

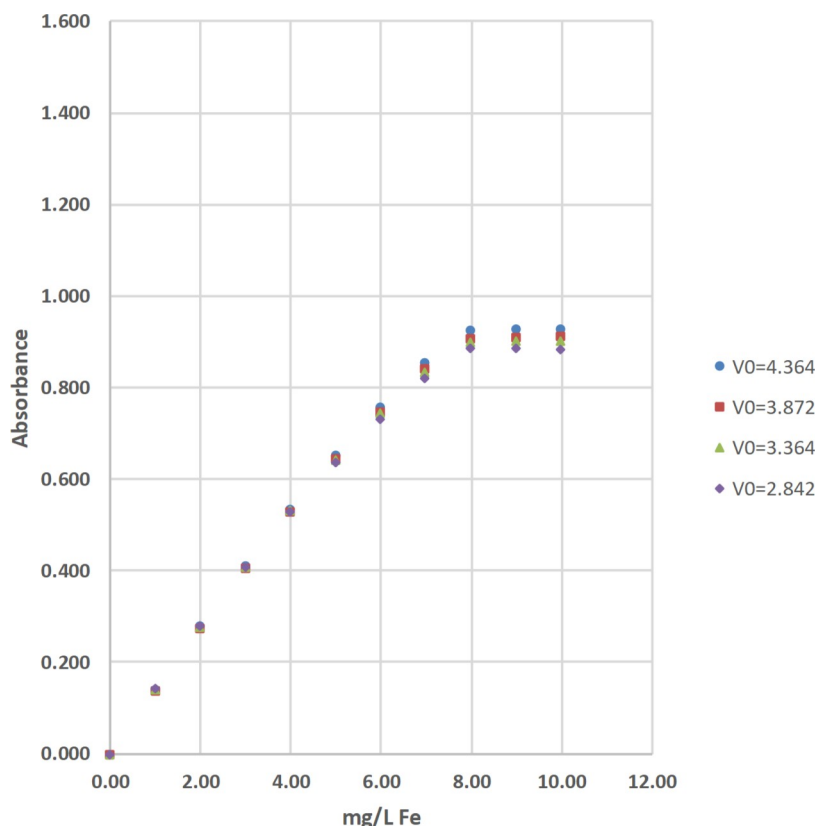https://doi.org/10.1371/journal.pone.0226761.g008

Fig 9. The calibration results for the determination of total iron (Fe) by the 1,10-phenanthroline method using light emitting diode (LED) spectrophotometer #1 at blank voltages (V_0) = 4.364 V, 3.872 V, 3.364 V, and 2.842 V [36].

Total fluoride (F⁻) by the sodium 2-(parasulfophenylazo)-1,8-dihydroxy-3,6-naphthalene disulfonate method

The concentrations of total fluoride (F^-) were determined by the sodium 2-(parasulfophenylazo)-1,8-dihydroxy-3,6-naphthalene disulfonate (SPADNS) method [36]. The absorbance of residual acid-zirconyl-SPADNS dye after the removal of colorless zirconium hexafluoride (ZrF_6^{2-}(aq, aqueous)) was measured at 567 nm with an Agilent Technologies Cary 60-UV-Vis (ultraviolet-visible) absorption spectrophotometer, and a LED spectrophotometer (Table 4; Figs 13 and 14). Standard solutions at 0.000, 0.201, 0.400, 0.601, 0.800, 1.000, 1.200, 1.399, 1.599, 1.800, and 2.000-mg/L of total F^-(aq) were used to calculate linear range [25], operational range [36], and calibration sensitivity [6, 38]. Seven 0.000-mg/L standard solutions were analyzed as samples and used to calculate the precision of standards [36], and the estimated limit of detection [26]. Lastly, a 0.600-mg/L standard solution was analyzed as a sample and used to calculate the % calibration check standard recovery [36]. This work was done at the Indian Institute of Science (IISc) in Bangalore using the same LED spectrophotometer #1 that was used for the determinations of total Fe and total Mn at Norwich University in Northfield, VT.

Adjusting blank voltage

The LED spectrophotometers use a variable resistor to adjust the voltage supplied to the LED (Table 1; Figs 3 and 5). This voltage (V_0, or the blank voltage) controls the brightness of the LED and was adjusted with a 0.00-mg/L Fe, 0.000-mg/L Mn, or 0.000-mg/L F^- standard in the
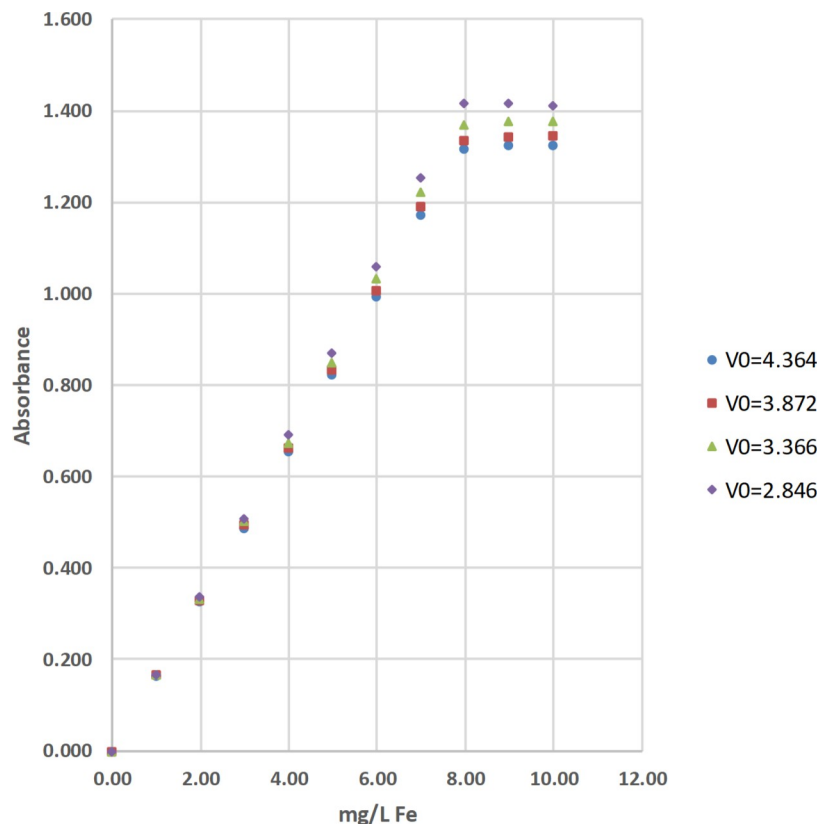
Fig 10. The calibration results for the determination of total iron (Fe) by the 1,10-phenanthroline method using light emitting diode (LED) spectrophotometer #2 at blank voltages (V_0) = 4.364 V, 3.872 V, 3.366 V, and 2.846 V [36].

sample cell holder (Figs 3 and 6). After it is adjusted, V_0 is held constant until all of the standards and samples in the analytical sequence are analyzed. For the total Fe and total Mn analyses in this study, 4 different values of V_0; that is, 4 different analytical sequences were used to evaluate the performance of a LED spectrophotometer and method (Tables 2 and 3; Figs 9, 10 and 12). More specifically, V_0 was initially set at or near its maximum voltage, then decreased in approximately 0.5-volt (V) increments until 4 different analytical sequences were performed (Tables 2 and 3; Figs 9, 10 and 12). For the total F^- analyses in this study, 6 different values of V_0; that is, 6 different analytical sequences were used to evaluate the performance of a LED spectrophotometer and method (Table 4; Fig 14). More specifically, V_0 was initially set at or near its maximum voltage, then decreased in approximately 0.05-volt (V) increments until 6 different analytical sequences were performed (Table 4; Fig 14).

Calculating absorbance

Two Fluke 175-True RMS Digital Multimeters were used to measure the voltages from the 2 LED spectrophotometers at Norwich University in Northfield, VT (Figs 3 and 7). A Haoyue DT830D Digital Multimeter was used to measure the voltages from the LED spectrophotometer at the Indian Institute of Science (IISc) in Bangalore. Eq 5 was used to convert these voltages to absorbances [39].

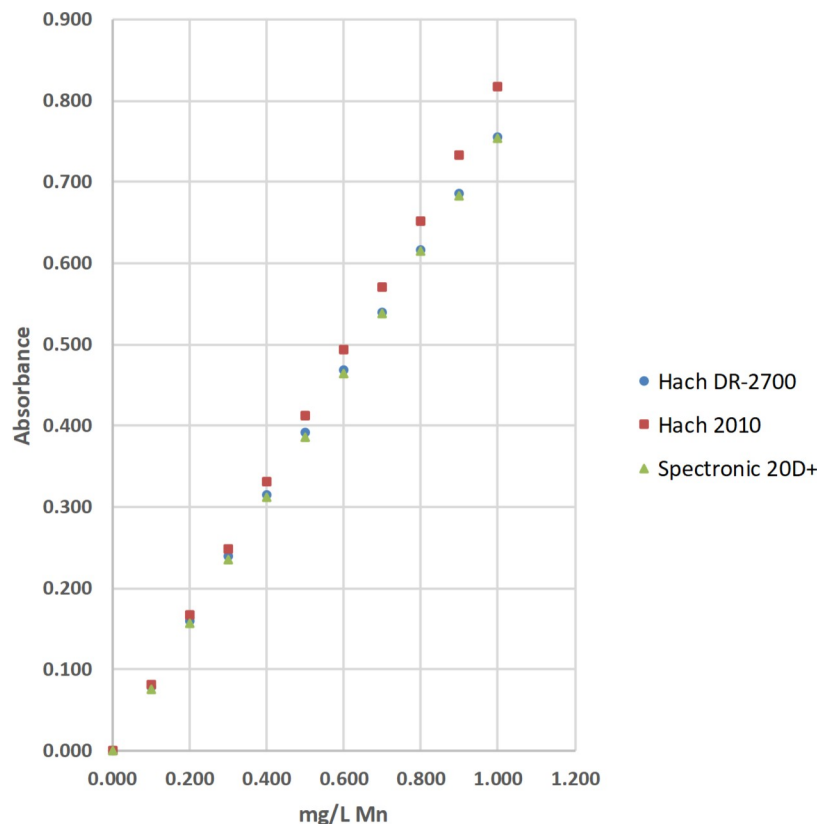$$A \approx \log_{10} \frac{V_0}{V} \tag{5}$$

Fig 11. The calibration results for the determination of total manganese (Mn) by the 1-(2-pyridylazo)-2-naphthol (PAN) method using a Hach DR-2700, a Hach 2010, and a Thermal Electron Spectronic 20D+ spectrophotometer [37].

https://doi.org/10.1371/journal.pone.0226761.g011

Where A is the absorbance, V_0 is the voltage with a 0.00-mg/L Fe, 0.000-mg/L Mn, or 0.000-mg/L F$^-$ standard in the sample cell holder, and V is the voltage with a sample in the sample cell holder (Figs 3 and 6).

Results and discussion

Price

The price in current (2019) USD of the 4 commercial spectrophotometers used in this study ranged from $2,424 to $7,644 (Tables 2–4). In contrast, the price in current (2019) USD for a LED spectrophotometer is $63 for parts (Tables 2–4). The commercial spectrophotometers are significantly more expensive than the LED spectrophotometer (Tables 2–4).

The $63 price of our LED spectrophotometer includes a single LED source assembly, and does not include the labor, overhead, and profit costs of the commercial spectrophotometers. Moreover, the LED spectrophotometer uses a simpler and less costly optical system. The LED spectrophotometer optical source costs approximately $3.27 for the source LED ($0.32), a 3.5-mm stereo male-male cable ($0.57), 1/8-inch heat shrink tubing ($0.10), and Sugru moldable glue ($2.28; Table 1). In contrast, a typical commercial spectrophotometer uses a more complicated and costly optical source. A typical commercial spectrophotometer might use a tungsten filament lamp, a field lens, a wavelength selector (an entrance slit, objective lens, diffraction grating, wavelength adjustment cam and actuator, light controller, occluder, and exit slit), a filter, and a measuring phototube [40]. As a result, our LED spectrophotometer uses a
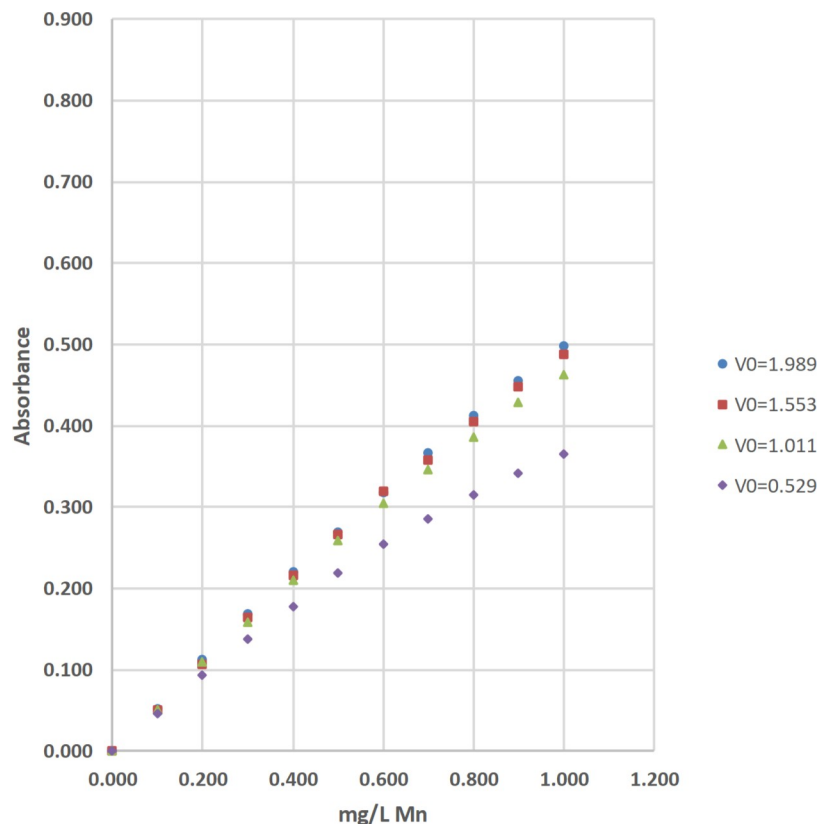
Fig 12. The calibration results for the determination of total manganese (Mn) by the 1-(2-pyridylazo)-2-naphthol (PAN) method using light emitting diode (LED) spectrophotometer #1 at blank voltages (V$_0$) = 1.989 V, 1.553 V, 1.011 V, and 0.529 V [37].

narrow range of polychromatic light with a spectral width of about 25 nm for a 510-nm source LED (Table 1). In contrast, commercial spectrophotometers use nearly monochromatic light [6]. Therefore, our spectrophotometer is less selective and more prone to interferences than a commercial spectrophotometer. Considering this limitation, it is imperative that users of our LED spectrophotometer be careful to avoid interferences by carefully monitoring the % recovery of known additions of standard to samples [1, 5, 36]. A known addition of standard to sample is also called a laboratory fortified sample matrix (LFSM), laboratory fortified matrix (LFM), or matrix spike (MS) [41]. Fortunately, this is standard operating procedure (SOP) in many routine drinking water testing laboratories [36, 41].

Calibration

Visual inspection and R^2 value of calibration curves. Calibration curves are used in spectrophotometry to determine the concentrations of analytes in samples. In this study, the concentration of total Fe, total Mn, or total F⁻ was the independent variable and was plotted on the x-axis. The absorbance was the dependent variable and was plotted on the y-axis (Figs 8–14). Calibration curves of the 1,10-phenanthroline method for total Fe and the 1-(2-pyridylazo)-2-naphthol (PAN) method for total Mn have positive slopes (Figs 8–12) [36, 37]. In contrast, calibration curves of the sodium 2-(parasulfophenylazo)-1,8-dihydroxy-3,6-naphthalene disulfonate (SPADNS) method for total F⁻ have negative slopes (Figs 13 and 14) [36].
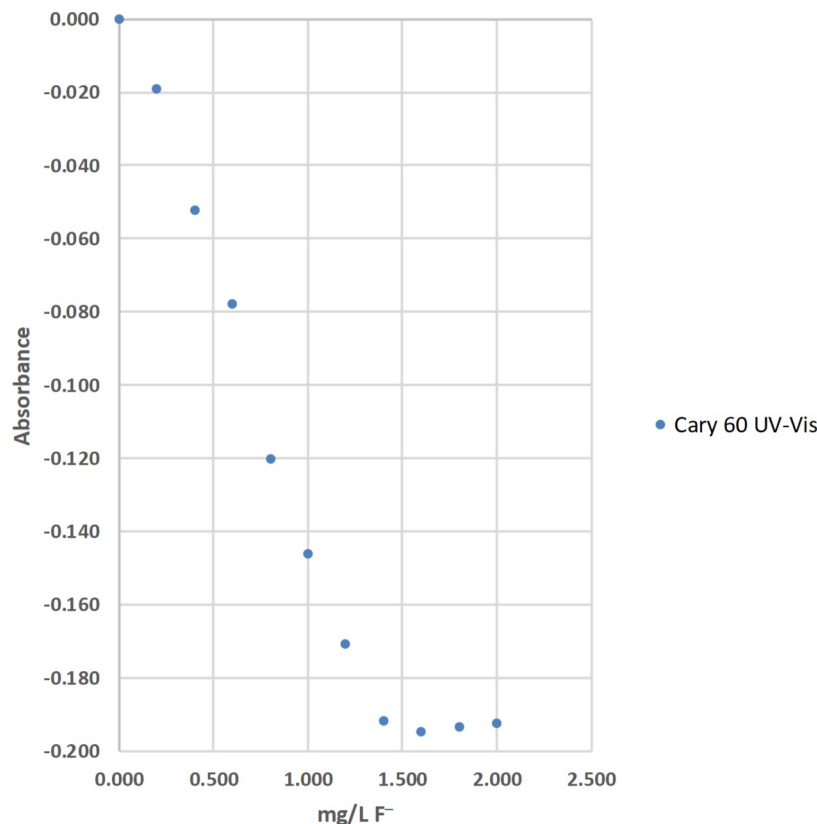
Fig 13. The calibration results for the determination of total fluoride (F⁻) by the sodium 2-(parasulfophenylazo)-1,8-dihydroxy-3,6-naphthalene disulfonate (SPADNS) method using an Agilent Technologies Cary 60 UV-Vis (ultraviolet-visible) absorption spectrophotometer [36].

According to the Beer-Bouguer-Lambert law, more commonly called Beer's law, at relatively low analyte concentrations, a linear calibration curve with the y-intercept going through the origin (0, 0) is expected [40]. For analyses with positive slopes and at relatively high analyte concentrations, little or no light from the source passes through the standard solutions and reach the detector; this causes a flattening of the calibration curve (Figs 8–10). For analyses with negative slopes and at relatively high analyte concentrations, an excess of light from the source passes through the standard solutions and reach the detector; this also causes a flattening of the calibration curve (Figs 13 and 14). Therefore, it is important to know the linearity and linear range for every method that is used on a given spectrophotometer. Historically, the linearity and the upper limit of linear range of calibration curves was subjectively evaluated by visual inspection (Figs 8–14).

A plot of R^2 values for each calibration curve in this study is shown in Fig 15. These R^2 values were used to subjectively evaluate the linearity of the 4 commercial and 2 LED spectrophotometers in this study (Fig 15). These calibration curves used linear regression through the origin for the 4 lowest concentration standards of each analyte (Tables 2–4).

The R^2 values ranged from 0.98948 to 1.00000 (Fig 15). These relatively large R^2 values suggest that all the calibration curves in this study are linear, especially considering that the calibration standard solutions have 3 significant figures. However, the importance of objectively testing the linearity of calibration curves is shown in the following example in which R^2 values are not associated with the linearity of the calibration curves (Table 4; Fig 15). The calibration
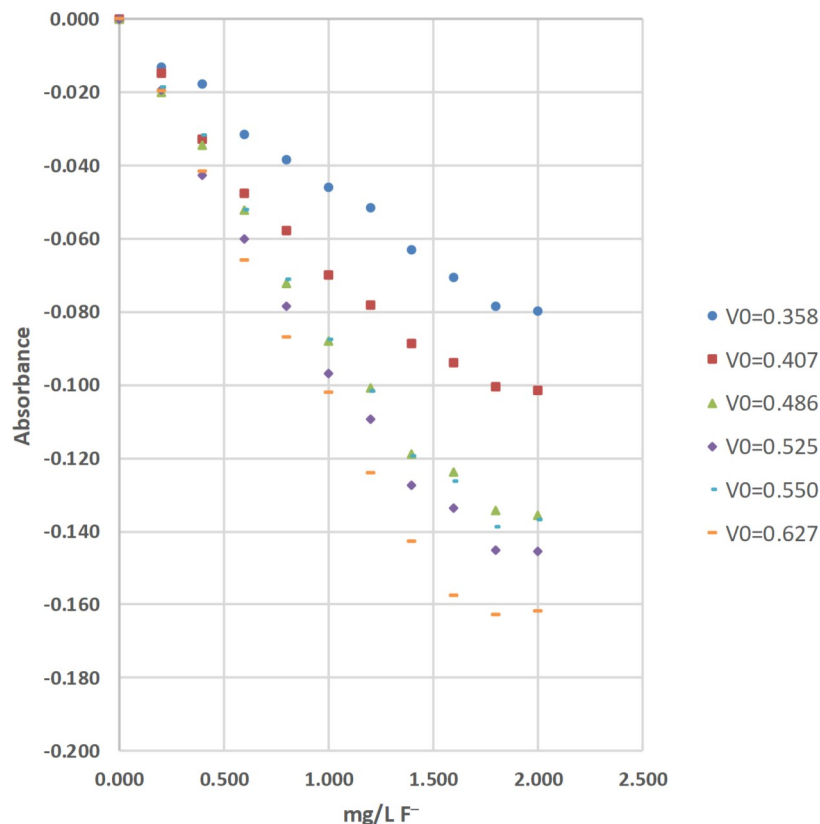
Fig 14. The calibration results for the determination of total fluoride (F⁻) by the sodium 2-(parasulfophenylazo)-1,8-dihydroxy-3,6-naphthalene disulfonate (SPADNS) method using light emitting diode (LED) spectrophotometer #1 at blank voltages (V_0) = 0.358 V, 0.407 V, 0.486 V, 0.525 V, 0.550 V, and 0.627 V [36].

https://doi.org/10.1371/journal.pone.0226761.g014

curve for LED spectrophotometer #1 at V_0 = 0.627 V had a statistically significant quadratic effect at the 95% confidence level (p-value = 0.0251); therefore, this calibration curve is non-linear despite having a relatively large R^2 (0.99876). In contrast, LED spectrophotometer #1 at V_0 = 0.358 V did not have a statistically significant quadratic effect at the 95% confidence level (p-value = 0.605); therefore, this calibration curve is linear despite having the smallest R^2 in the study (0.98948). In this example, the calibration curve with the larger R^2 is nonlinear and the calibration curve with the smaller R^2 is linear. This limitation of using R^2 as a subjective test of linearity is well known in analytical chemistry [42].

Upper limit of linear range. This paper demonstrates the novel use of objective tests for higher order polynomial relationships to measure the upper limits of linear range (Tables 2–4) [25]. These objective measurements of the upper limits of linear range greatly influenced the many design decisions that were made during the 3-year design and testing phase of this project.

Polynomial regression was used to objectively calculate the linear range of each calibration curve in this study (Tables 2, 3 and 4; Figs 8–14) [25]. Since Beer's law says that a linear calibra-tion curve is expected, a regression of absorbance on the concentration of analyte and the con-centration of analyte squared was used to test the significance of a second-order or quadratic effect [25]. If this quadratic effect was statistically significant at α = 0.05, the calibration curve is not linear at the 95% confidence level [25]. In contrast, if this quadratic effect was not statis-tically significant, the calibration curve is linear [25].
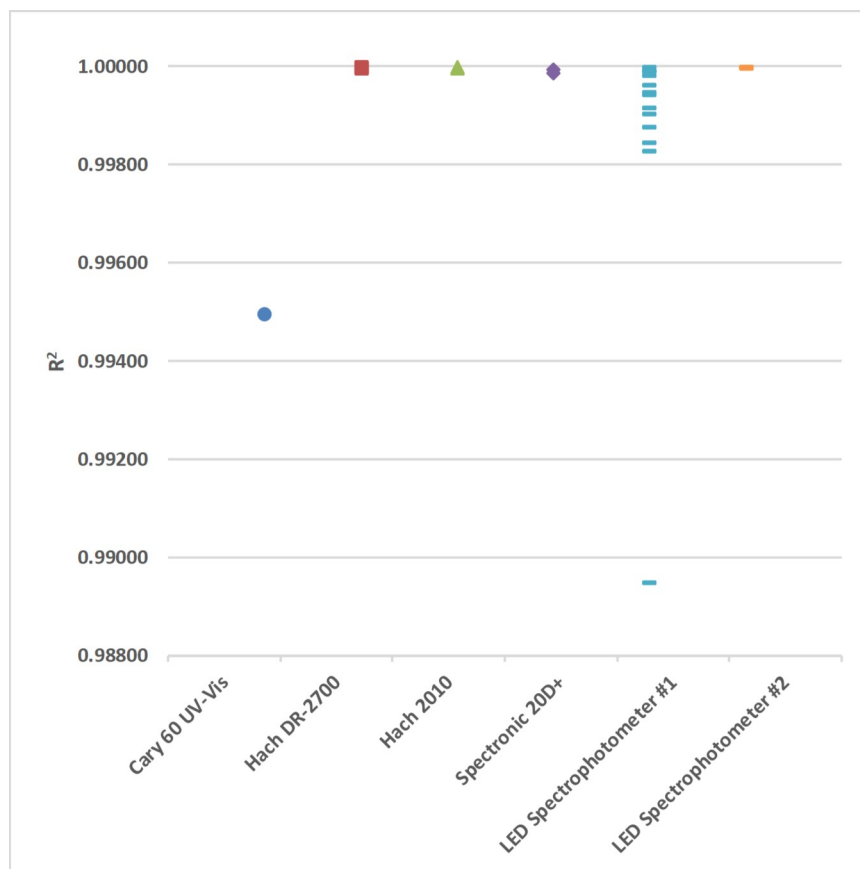
Fig 15. The R^2 values for the Agilent Technologies Cary 60 UV-Vis (ultraviolet-visible), Hach DR-2700, a Hach 2010, a Thermal Electron Spectronic 20D+, and 2 light emitting diode (LED) spectrophotometers used in this study (Tables 2–4).

At least 4 different concentrations of standard solution are required to test for a quadratic effect [43]. Therefore, the absorbances from the 4 lowest concentrations of standard solutions were tested for a significant quadratic effect [25]. If this quadratic effect was not statistically significant, the calibration curve is linear and the process was repeated with the absorbances from the 5 lowest concentrations of standard solutions [25]. This process continued until the quadratic effect was statistically significant [25].

For example, the regression of absorbance (0.000, 0.178, 0.349, and 0.521) on the respective concentration of total Fe (0.00, 1.01, 2.00, and 3.00 mg/L) and the respective concentration of total Fe squared (0.00, 1.02, 3.99, and 8.97 $(mg/L)^2$) was used to test the significance of a quadratic effect for the Hach DR-2700 (Table 2; Fig 8). The results of this first regression are shown in Eq 6.

$$\text{Absorbance} = -9.86 \times 10^{-4}(mg/L)^2 + 0.177(mg/L) + 1.51 \times 10^{-4} \qquad (6)$$

The quadratic effect coefficient (-9.86×10^{-4}) is equivalent to 0 at the 95% confidence level (p-value = 0.213). It has a 95% confidence interval that includes 0; this interval extends from -5.34×10^{-3} to 3.37×10^{-3}. This conclusion suggests that the calibration curve is linear, so the process was repeated with the 0.00, 1.01, 2.00, 3.00, and 3.99-mg/L standard solutions. The absorbance equaled 0.686 at 3.99 mg/L and 15.94 $(mg/L)^2$. The results of this second regression

are shown in Eq 7.

$$\text{Absorbance} = -1.60 \times 10^{-3}(\text{mg/L})^2 + 0.178(\text{mg/L}) - 2.15 \times 10^{-4} \tag{7}$$

In contrast, the quadratic effect coefficient (-1.60×10^{-3}) is different from 0 at the 95% confidence level (p-value = 0.0343). It has a 95% confidence interval that does not include 0; this interval extends from -2.91×10^{-3} to -2.91×10^{-4}. This conclusion suggests that the calibration curve is not linear, so the process was stopped and the upper limit of the linear range was set at 3.00 mg/L total Fe (Table 2; Fig 8).

The upper limits of linear range for the 3 commercial spectrophotometers used in the United States extended from 3.00 to 6.99 mg/L for total Fe (Table 2; Fig 8). By comparison, the upper limits of linear range for the 2 LED spectrophotometers extended from 3.00 to 4.99 mg/L for total Fe (Table 2; Figs 9 and 10). The upper limits of linear range for the 3 commercial spectrophotometers used in the United States extended from 0.500 to 0.700 mg/L for total Mn (Table 3; Fig 11). By comparison, the upper limits of linear range for the LED spectrophotometer extended from 0.400 to 0.600 mg/L for total Mn (Table 3; Fig 12). The upper limit of linear range for the 1 commercial spectrophotometer used in India was 1.599 mg/L for total F^- (Table 4; Fig 13). By comparison, the upper limits of linear range for the LED spectrophotometer extended from 0.000 (nonlinear) to 1.800 mg/L for total F^- (Table 4; Fig 14). The small blank voltages (V_0) of the total F^- analyses most likely gave small signal to noise ratios and the large spread of upper limits of linear range for the LED spectrophotometer (Table 4; Fig 14). Even so, these results suggest that the LED spectrophotometers have upper limits of linear range that are generally comparable to those of the 4 commercial spectrophotometers used in this study (Tables 2–4; Figs 8–14) and would be sufficient for comparisons to World Health Organization (WHO) guidelines for drinking water quality or health-based values for these analytes [44, 45].

Upper limit of operational range. The operational or calibration range must be determined "before using a new method or instrument", according to the American Public Health Association (APHA), American Water Works Association (AWWA), and Water Environment Federation (WEF) [36]. These organizations say that both linear and nonlinear regions of a calibration curve can be used in routine drinking water testing laboratories [36]. Moreover, these organizations allow individual laboratories to make their own definition of operational range [36]. That is, there is no standard definition of operational range.

For this study, the upper limit of operational range was defined by the last change in the absorbance of incremental standards that is 50% less than the change in the absorbance of the corresponding 0.00- and 1.01-mg/L total Fe standards, the corresponding 0.00- and 0.100-mg/L total Mn standards, or the corresponding 0.000- and 0.201-mg/L of total F^- standards (Tables 2–4; Figs 8–14). For example, the Hach DR-2700 gave absorbances of 0.000, 0.178, 1.169, 1.286, and 1.293 for the 0.00, 1.01, 6.99, 7.98, and 8.98-mg/L total Fe standards, respectively. The % change in absorbance for the 6.99- and 7.98-mg/L total Fe standards relative to the 0.00- and 1.01-mg/L total Fe standards is shown in Eq 8.

$$\frac{\text{Relative}}{\text{Change}} = \frac{(1.286 - 1.169)}{(0.178 - 0.000)} \times 100\% = 65.7\% \tag{8}$$

In contrast, the % change in absorbance for the 7.98- and 8.98-mg/L total Fe standards relative to the 0.00- and 1.01-mg/L total Fe standards is shown in Eq 9.

$$\frac{\text{Relative}}{\text{Change}} = \frac{(1.293 - 1.286)}{(0.178 - 0.000)} \times 100\% = 3.93\% \tag{9}$$

Therefore, the upper limit of the operational range was set at 7.98 mg/L total Fe (Table 2; Fig 8).

The upper limits of operational range for the 3 commercial spectrophotometers used in the United States and LED spectrophotometer #2 equaled 7.98 mg/L for total Fe (Table 2; Figs 8 and 9). By comparison, the upper limit of operational range for LED spectrophotometer #1 equaled 6.99 mg/L for total Fe (Table 2; Fig 9). The upper limits of operational range for all of the spectrophotometers was greater than or equal to ($\geq$) 1.000 mg/L for total Mn (Table 3; Figs 11 and 12). The upper limit of operational range for the 1 commercial spectrophotometer used in India was 1.399 mg/L for total F$^-$ (Table 4; Fig 13). By comparison, the upper limits of operational range for the LED spectrophotometer extended from 0.201 to 1.599 mg/L for total F$^-$ (Table 4; Fig 14). The small blank voltages (V_0) of the total F$^-$ analyses most likely gave small signal to noise ratios and the large spread of upper limits of operational range for the LED spectrophotometer (Table 4; Fig 14). Even so, these results suggest that the LED spectrophotometers have upper limits of operational range that are generally comparable to those of the 4 commercial spectrophotometers used in this study (Tables 2–4; Figs 8–14) and would be sufficient for comparisons to WHO guidelines for drinking water quality or health-based values for these analytes [44, 45].

Calibration sensitivity and R^2.   Sensitivity is the ability to discriminate between small differences in analyte concentration [6]. More specifically, calibration sensitivity is the slope of a calibration curve [6]. That is, it is the change in absorbance per unit change in concentration. Therefore, the larger the slope, the larger the calibration sensitivity. The slope equals the absorptivity constant, a, which depends on the wavelength and the nature of the absorbing compound, multiplied by the path length through the absorbing compound, b [40]. This is Beer's law and is shown in Eq 10 [40].

$$A = abc = \log_{10} \frac{P_0}{P} \tag{10}$$

The absorbance, A, equals this slope (ab) multiplied by the concentration of absorbing compound, c [40]. The absorbance, A, also equals the log base 10 of the power of monochromatic light entering the sample, P_0, divided by the power of monochromatic light leaving the sample, P (Eq 10) [40]. Therefore, absorbance is a unitless ratio. In contrast, the units of slope or calibration sensitivity are L/mg.

For this study, calibration sensitivity was defined as the absolute value of the slope of a calibration curve using linear regression through the origin for the 0.00, 1.01, 2.00, and 3.00-mg/L standards for Fe (Table 2; Figs 8–10), for the 0.000, 0.100, 0.200, and 0.300-mg/L standards for Mn (Table 3; Figs 11 and 12), and for the 0.000, 0.201, 0.400, and 0.601-mg/L standards for F$^-$ (Table 4; Figs 13 and 14). These calibration sensitivities and the R^2 values for these linear regressions through the origin are shown in Tables 2–4.

The calibration sensitivities for the 3 commercial spectrophotometers used in the United States ranged from 0.165 to 0.180 L/mg for total Fe (Table 2; Fig 8). The R^2 values for these regressions ranged from 0.99994 to 1.00000 (Table 2; Fig 8). By comparison, the calibration sensitivities for the 2 LED spectrophotometers ranged from 0.136 to 0.169 L/mg for total Fe (Table 2; Figs 9 and 10). The R^2 values for these regressions ranged from 0.99980 to 0.99999 (Table 2; Figs 9 and 10).

The calibration sensitivities for the 3 commercial spectrophotometers used in the United States ranged from 0.781 to 0.828 L/mg for total Mn (Table 3; Fig 11). The R^2 values for these regressions ranged from 0.99987 to 0.99997 (Table 3; Fig 11). By comparison, the calibration sensitivities for the LED spectrophotometer ranged from 0.463 to 0.558 L/mg for total Mn

(Table 3; Fig 12). The R^2 values for these regressions ranged from 0.99943 to 0.99990 (Table 3; Fig 12).

The calibration sensitivity for the 1 commercial spectrophotometer used in India was 0.127 L/mg for total F^- (Table 4; Fig 13). The R^2 for this regression was 0.99494 (Table 4; Fig 13). By comparison, the calibration sensitivities for the LED spectrophotometer ranged from 0.051 to 0.107 L/mg for total F^- (Table 4; Fig 14). The R^2 values for these regressions ranged from 0.98948 to 0.99914 (Table 4; Fig 14).

These results suggest that the LED spectrophotometers have calibration sensitivities that are in general slightly less than, but still comparable to those of the 4 commercial spectrophotometers used in this study (Tables 2–4). The maximum V_0 of LED spectrophotometer #1 decreased significantly from approximately 4.364 V with the 510-nm LED (32 milliwatt/steradian; mW/sr) for total Fe, to 1.989 V with the 560-nm LED (0.022 mW/sr) for total Mn, and to 0.627 V with the 567-nm LED (0.73 mW/sr) for total F^- (Tables 2–4). This decrease in V_0 is the most likely cause of this decrease in the calibration sensitivities of the LED spectrophotometers. If so, radiant intensity is an important criteria for selecting a source LED.

Moreover, the 2 LED spectrophotometers were made from the same components; however, the slight difference in the calibration sensitivities of these instruments for total Fe might result from slight differences in the performance of these components (Table 2; Figs 9 and 10).

Precision

In analytical chemistry, precision is the agreement between repeated measurements of the same standard, known addition of standard to sample, or sample [36]. More specifically, the precision of standards is usually expressed as a sample standard deviation, s [46]. In this study, the precision of standards equals s for the 7 separately prepared 0.00-mg/L Fe standards that were analyzed as samples, the 7 separately prepared 0.000-mg/L Mn standards that were analyzed as samples, or the 7 separately prepared 0.000-mg/L F^- standards that were analyzed as samples.

The precisions of standards for the 3 commercial spectrophotometers used in the United States ranged from 0.002 to 0.003 mg/L for total Fe (Table 2). By comparison, the precisions of standards for the 2 LED spectrophotometers ranged from 0.003 to 0.009 mg/L for total Fe (Table 2). The precisions of standards for the 3 commercial spectrophotometers used in the United States ranged from 0.0006 to 0.003 mg/L for total Mn (Table 3). By comparison, the precisions of standards for the LED spectrophotometer ranged from 0.001 to 0.005 mg/L for total Mn (Table 3). These results suggest that for total Fe and total Mn analyses, the LED spectrophotometers have precisions of standards that are in general slightly greater than, but still comparable to those of the 3 commercial spectrophotometers used in the United States (Tables 2 and 3). This conclusion is in agreement with that for the calibration sensitivities (Tables 2 and 3).

The precision of standards for the 1 commercial spectrophotometer used in India was 0.01 mg/L for total F^- (Table 4). By comparison, the precisions of standards for the LED spectrophotometer ranged from 0.005 to 0.03 mg/L for total F^- (Table 4). These results suggest that the LED spectrophotometer has precisions of standards that are generally comparable to those of the 1 commercial spectrophotometer used in India (Table 4).

Limit of detection

The limit of detection is the smallest concentration that can be detected with reasonable certainty for a given analytical procedure [47]. There are many different ways to calculate limit of detection [48]. For this study, the estimated limit of detection was based on a 1-tailed 99%

confidence interval from the 7 separately prepared 0.00-mg/L Fe standards that were analyzed as samples, the 7 separately prepared 0.000-mg/L Mn standards that were analyzed as samples, or the 7 separately prepared 0.000-mg/L F⁻ standards that were analyzed as samples. This approach, called the method detection limit based on control charts, typically uses the results from many days, or even over all days that samples are analyzed [26]. Since this study used 1 day of analysis for each analyte, instead of the weeks, months, or even years of analyses used by the method detection limit based on control charts the sample mean, $\bar{X}$, for this study was set to 0 mg/L so that the resulting estimated limits of detection are comparable. This 1 day of analysis and setting $\bar{X}$ to 0 mg/L are why the resulting limits of detection are named estimated limits of detection in this study.

The estimated limits of detection for the 3 commercial spectrophotometers used in the United States ranged from 0.003 to 0.004 mg/L for total Fe (Table 2). By comparison, the estimated limits of detection for the 2 LED spectrophotometers ranged from 0.004 to 0.010 mg/L for total Fe (Table 2). The estimated limits of detection for the 3 commercial spectrophotometers used in the United States ranged from 0.0007 to 0.003 mg/L for total Mn (Table 3). By comparison, the estimated limits of detection for the LED spectrophotometer ranged from 0.001 to 0.006 mg/L for total Mn (Table 3). These results suggest that for total Fe and total Mn analyses, the LED spectrophotometers have estimated limits of detection that are in general slightly greater than, but still comparable to those of the 3 commercial spectrophotometers used in the United States (Tables 2 and 3). This conclusion is in agreement with that for the precisions of standards and the calibration sensitivities (Tables 2 and 3).

The estimated limit of detection for the 1 commercial spectrophotometer used in India was 0.01 mg/L for total F⁻ (Table 4). By comparison, the estimated limits of detection for the LED spectrophotometer ranged from 0.006 to 0.03 mg/L for total F⁻ (Table 4). These results suggest that the LED spectrophotometer has estimated limits of detection that are generally comparable to those of the 1 commercial spectrophotometer used in India (Table 4) and would be sufficient for comparisons to WHO guidelines for drinking water quality or health-based values for these analytes [44, 45].

Instrument stability

A calibration check standard is a standard that is analyzed as a sample; typically, after every 10 samples and after the last sample are analyzed [36]. Calibration check standards are used to monitor the stability of the instrument and the method during the analysis of samples [36]. Ideally, the % calibration check standard recovery is 100% plus or minus an acceptable random error [36]. This error is often determined in routine drinking water testing laboratories by control charts; running 95% or 99% confidence intervals of the measured concentration or % recovery of the calibration check standards plotted on the y-axis, and the date of analysis plotted on the x-axis [36].

If a control chart of % calibration check standard recovery is not available, then a range of 100±15% calibration check standard recovery is acceptable [49]. All the % calibration check standard recoveries in this study are well within this 85-to-115% acceptable range (Tables 2–4).

The % calibration check standard recoveries for the 3 commercial spectrophotometers used in the United States ranged from 99.6 to 99.8% for total Fe (Table 2). By comparison, the % calibration check standard recoveries for the 2 LED spectrophotometers ranged from 98.8 to 100.0% for total Fe (Table 2). The % calibration check standard recoveries for the 3 commercial spectrophotometers used in the United States ranged from 98.8 to 107.7% for total Mn (Table 3). By comparison, the % calibration check standard recoveries for the LED

spectrophotometer ranged from 98.3 to 99.2% for total Mn (Table 3). The % calibration check standard recovery for the 1 commercial spectrophotometer used in India was 96.8% for total F^- (Table 4). By comparison, the % calibration check standard recovery for the LED spectrophotometer ranged from 100.0 to 104.0% for total F^- (Table 4). These results suggest that the LED spectrophotometers have % calibration check standard recoveries that are generally comparable to those of the 4 commercial spectrophotometers used in this study (Tables 2–4) and would be sufficient for comparisons to WHO guidelines for drinking water quality or health-based values for these analytes [44, 45].

Bland-Altman comparison

Bland-Altman plots for pair-wise comparisons of LED spectrophotometer #1 with 3 commercial spectrophotometers (Hach DR-2700, Hach 2010, Thermal Electron Spectronic 20D+) for Fe and Mn, as well as for LED spectrophotometer #1 with Agilent Technologies Cary 60 UV-Vis for F^- are presented in Figs 16–22 [50].

LED spectrophotometer #1 was selected for these comparisons since it was used to measure every analyte (Tables 2–4). These comparisons were made with the LED spectrophotometer set at its maximum blank voltage (V_0; Tables 2–4). In each of these 7 comparisons, every point is within the lower and upper 95% confidence limits; therefore, the Bland-Altman plots show no statistically significant differences in the measurements made by the commercial spectrophotometers and LED spectrophotometer #1.

Conclusions

Our LED spectrophotometer costs $63 USD for parts (Table 1). The 4 commercial spectrophotometers in this study ranged in cost from $2,424 to $7,644 USD (Tables 2–4). That is, our LED spectrophotometer costs between 2.2 and 0.70% of the 4 commercial spectrophotometers. Clearly, our LED spectrophotometer is extremely affordable compared to these 4 commercial spectrophotometers.

The upper limits of linear range for our LED spectrophotometer ranged from 3.00 to 4.99 mg/L, 0.400 to 0.600 mg/L, and 0.000 to 1.800 mg/L for the determinations of Fe, Mn, and F^-,
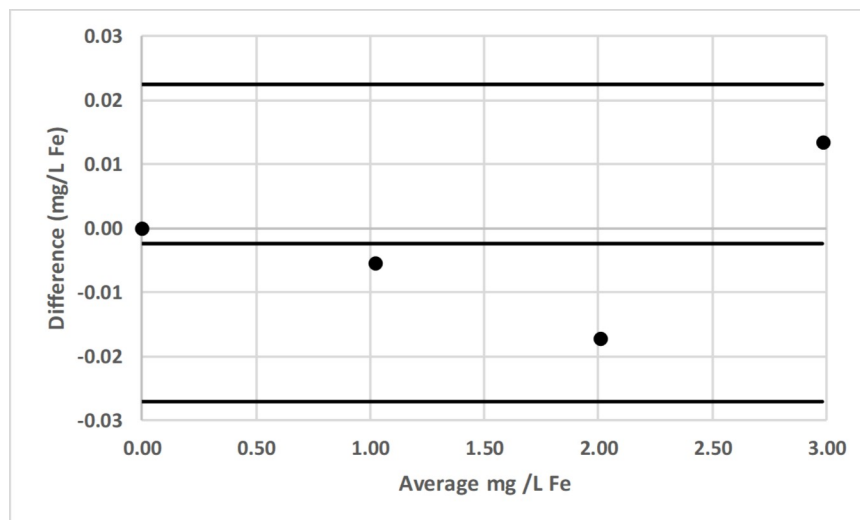

Fig 16. Bland-Altman plot comparing the Hach DR-2700 and LED spectrophotometer #1 for the determination of total iron (Fe) by the 1,10-phenanthroline method [36].
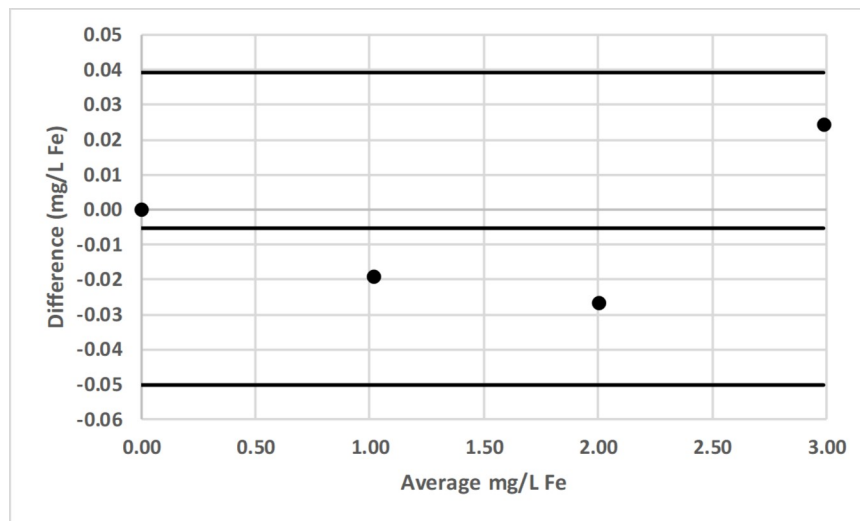
Fig 17. Bland-Altman plot comparing the Hach 2010 and LED spectrophotometer #1 for the determination of total iron (Fe) by the 1,10-phenanthroline method [36].

https://doi.org/10.1371/journal.pone.0226761.g017

respectively (Tables 2–4). By comparison, these limits for the 4 commercial spectrophotometers in this study ranged from 3.00 to 6.99 mg/L, 0.500 to 0.700 mg/L, and 1.599 mg/L for the determinations of Fe, Mn, and F⁻, respectively (Tables 2–4). That is, each of these 3 ranges for our LED spectrophotometer overlapped with each of the 3 corresponding ranges for the commercial spectrophotometers. Therefore, there is no practical difference in the upper limits of linear range for our LED spectrophotometer and the 4 commercial spectrophotometers in this study; therefore, our LED spectrophotometer would be sufficient for comparisons to WHO guidelines for drinking water quality or health-based values for these analytes [44, 45].

Similarly, there are no practical differences in the upper limits of operational range, R^2 values, precisions of standards, and estimated limits of detection for our LED spectrophotometer and these 4 commercial spectrophotometers (Tables 2–4).
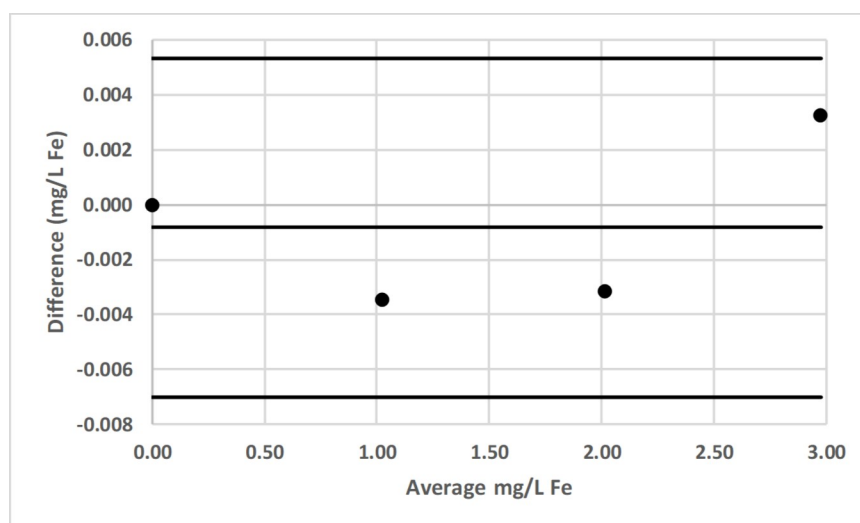

Fig 18. Bland-Altman plot comparing the Thermal Electron Spectronic 20D+ and LED spectrophotometer #1 for the determination of total iron (Fe) by the 1,10-phenanthroline method [36].

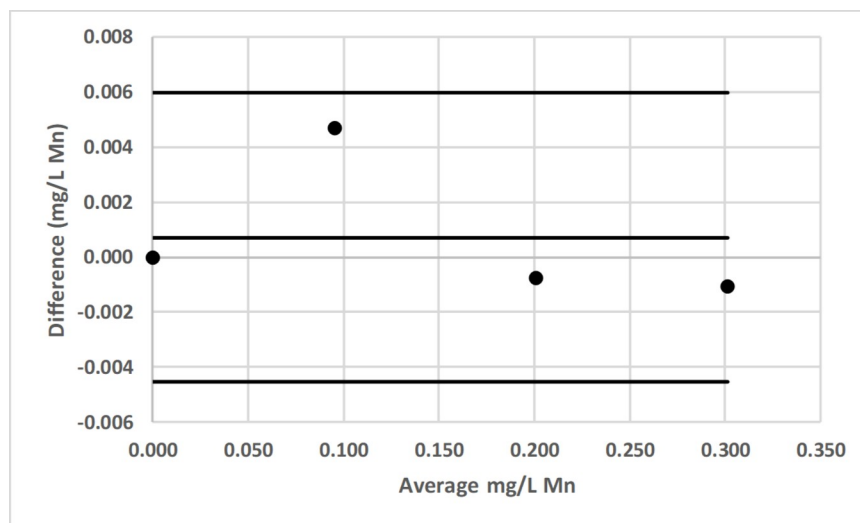https://doi.org/10.1371/journal.pone.0226761.g018

Fig 19. Bland-Altman plot comparing the Hach DR-2700 and LED spectrophotometer #1 for the determination of total manganese (Mn) by the Hach 1-(2-pyridylazo)-2-naphthol (PAN) method [37].

There is no practical difference in the calibration sensitivity for our LED spectrophotometer and these 4 commercial spectrophotometers for the determination of Fe; however, there is a practical difference in the calibration sensitivities for our LED spectrophotometer and these 4 commercial spectrophotometers for the determinations of Mn and F⁻ (Tables 2–4). More specifically, the % of the average calibration sensitivity for our LED spectrophotometer divided by the average calibration sensitivity for these 4 commercial spectrophotometers are 87.7, 65.2, and 67.0% for the determinations of Fe, Mn, and F⁻, respectively (Tables 2–4).

In conclusion, this paper describes the design, use, and performance of an extremely affordable, and sufficiently accurate and precise LED spectrophotometer for drinking water and other testing in regions with limited resources.
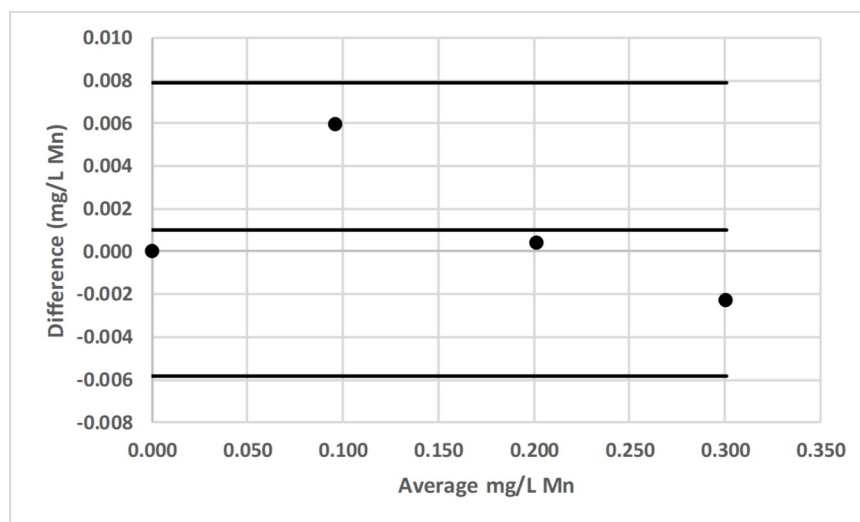

Fig 20. Bland-Altman plot comparing the Hach 2010 and LED spectrophotometer #1 for the determination of total manganese (Mn) by the Hach 1-(2-pyridylazo)-2-naphthol (PAN) method [37].
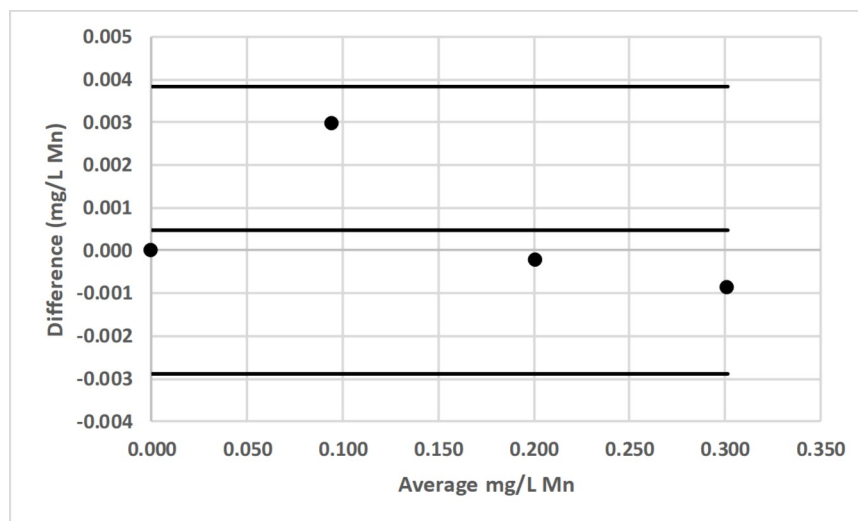
Fig 21. Bland-Altman plot comparing the Thermal Electron Spectronic 20D+ and LED spectrophotometer #1 for the determination of total manganese (Mn) by the Hach 1-(2-pyridylazo)-2-naphthol (PAN) method [37].

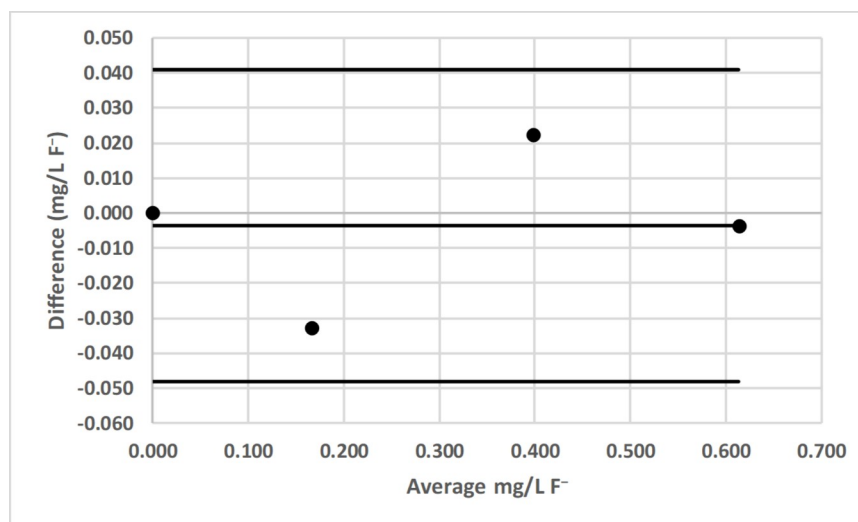https://doi.org/10.1371/journal.pone.0226761.g021

Fig 22. Bland-Altman plot comparing the Agilent Technologies Cary 60 UV-Vis and LED spectrophotometer #1 for the determination of total fluoride (F⁻) by the sodium 2-(parasulfophenylazo)-1,8-dihydroxy-3,6-naphthalene disulfonate (SPADNS) method [36].

https://doi.org/10.1371/journal.pone.0226761.g022

Supporting information

S1 Tables. Iron data and analysis.
(XLSX)

S2 Tables. Manganese data and analysis.
(XLSX)

S3 Tables. Fluoride data and analysis.
(XLSX)

S4 Tables. The combined iron, manganese, and fluoride data and analysis.
(XLSX)

Acknowledgments

Author Contributions

Conceptualization: Michael W. Prairie, Seth H. Frisbie, K. Kesava Rao.

Formal analysis: Seth H. Frisbie.

Investigation: Michael W. Prairie, Seth H. Frisbie, K. Kesava Rao, Anyamanee H. Saksri, Shreyas Parbat.

Methodology: Michael W. Prairie, Seth H. Frisbie, K. Kesava Rao.

Project administration: Michael W. Prairie, Seth H. Frisbie, K. Kesava Rao.

Resources: Michael W. Prairie, Seth H. Frisbie, K. Kesava Rao.

Supervision: Michael W. Prairie, Seth H. Frisbie, K. Kesava Rao.

Validation: Michael W. Prairie, Seth H. Frisbie, K. Kesava Rao.

Visualization: Michael W. Prairie, Seth H. Frisbie.

Writing – original draft: Seth H. Frisbie.

Writing – review & editing: Michael W. Prairie, Seth H. Frisbie, K. Kesava Rao, Anyamanee H. Saksri, Shreyas Parbat, Erika J. Mitchell.

References

1. Frisbie SH, Maynard DM, Hoque BA. The nature and extent of arsenic-affected drinking water in Bangladesh. In: Sarkar B, editor. Metals and genetics. New York, NY: Plenum Publishing Company; 1999. pp. 67–85.

2. United States Agency for International Development. Report of the impact of the Bangladesh Rural Electrification Program on groundwater quality. Prepared by the Bangladesh Rural Electrification Board. Funded by U.S. AID, Contract Number: U.S AID RE III 388–0070. Dhaka, Bangladesh: U.S. AID; 1997.

3. Tzanavarasa PD, Themelisb DG. Review of recent applications of flow injection spectrophotometry to pharmaceutical analysis. Anal Chim Acta. 2007; 588(1):1–9, https://doi.org/10.1016/j.aca.2007.01.060 PMID: 17386786, https://doi.org/10.1016/j.aca.2007.01.060

4. Bishop ML, Fody EP, Schoeff LE, editors. Clinical chemistry: Principles, techniques, and correlations. 7th ed. Philadelphia, PA: Lippincott Williams & Wilkins; 2013. pp. 101–106, 110–111, 157.

5. Frisbie SH, Ortega R, Maynard DM, Sarkar B. The concentrations of arsenic and other toxic elements in Bangladesh's drinking water. Environ Health Perspect. 2002; 110(11):1147–1153, https://doi.org/10.1289/ehp.021101147 PMID: 12417487, https://doi.org/10.1289/ehp.021101147

6. Skoog DA, Holler FJ, Crouch SR. Principles of instrumental analysis. 7th ed. Boston, MA: Cengage Learning; 2018. pp. 16–19, 142–143, 160–172, 304–340.

7. Thorlabs. Unmounted LEDs. 2019. Available from: https://www.thorlabs.com/newgrouppage9.cfm?objectgroup_id=2814 [accessed 20 October 2019].

8. Albert DR, Todt MA, Davis HF. A low-cost quantitative absorption spectrophotometer. J Chem Educ. 2012; 89(11):1432−1435, https://doi.org/10.1021/ed200829d

9. Asheim J, Kvittingen EV, Kvittingen L, Verley R. A simple, small-scale Lego colorimeter with a light-emitting diode (LED) used as detector. J Chem Educ. 2014; 91(7):1037−1039, https://doi.org/10.1021/ed400838n

10. Forbes PBC, Nöthling JA. Shedding light on spectrophotometry: The SpecUP educational spectropho- tometer. S Afr J Sci. 2014; 110(1/2), https://www.sajs.co.za/article/view/3659/4756

11. Kvittingen EV, Kvittingen L, Sjursnes BJ, Verley R. Simple and inexpensive UV-photometer using LEDs as both light source and detector. J Chem Educ. 2016; 93(10):1814−1817, https://doi.org/10.1021/acs.jchemed.6b00156

12. O'Donoghue J. Simplified low-cost colorimetry for education and public engagement. J Chem Educ. 2019; 96(6):1136−1142, https://doi.org/10.1021/acs.jchemed.9b00301

13. Place BJ. Activity analysis of iron in water using a simple LED spectrophotometer. J Chem Educ. 2019; 96(4):714−719, https://doi.org/10.1021/acs.jchemed.8b00515

14. Santos WG, Cavalheiro ÉTG. Assembling and using an LED-based detector to monitor absorbance changes during acid-base titrations. J Chem Educ. 2015; 92(10):1709−1715, https://doi.org/10.1021/ed500931p

15. Thal MA, Samide MJ. Applied electronics: Construction of a simple spectrophotometer. J Chem Educ. 2001; 78(11):1510, https://doi.org/10.1021/ed078p1510

16. Wilson MV, Wilson E. Authentic performance in the instrumental analysis laboratory: Building a visible spectrophotometer prototype. J Chem Educ. 2016; 94(1):44−51, https://doi.org/10.1021/acs.jchemed.6b00515

17. Mestha LK, Hubble III FF, Love TL, Skinner G, Mihalyov KJ, Robbins DA, Diehl DM. Low Cost LED Based Spectrophotometer. In: Final Program and Proceedings of ICIS '06, International Congress of Imaging Science. Rochester, NY: Society for Imaging Science and Technology; 2006. pp. 95−98.

18. Alam MAE, Islam MR, Faria IJ. Development and Validation of a Low-Cost Visible Light Spectrophotom- eter. In: Proceedings of the Fourth International Conference on Advances in Electrical Engineering. Dhaka, Bangladesh: Institute of Electrical and Electronics Engineers; 2017. pp. 653−657.

19. Chaianantakul N, Wutthi K, Kamput N, Pramanpol N, Janphuang P, Pummara W, Phimon K, Phattha- nakun R. Development of mini-spectrophotometer for determination of plasma glucose. Spectrochim Acta A. 2018; 204:670–676, https://doi.org/https://doi.org/10.1016/j.saa.2018.06.107

20. Gong W, Mowlem M, Kraft M, Morgan H. A simple, low-cost double beam spectrophotometer for colori- metric detection of nitrite in seawater. IEEE Sens J. 2009; 9(7):862–869, https://doi.org/10.1109/JSEN.2009.2020659

21. Lima KMG. A portable photometer based on LED for the determination of aromatic hydrocarbons in water. Microchem J. 2012; 103:62–67, https://doi.org/10.1016/j.microc.2012.01.003

22. Mohammad KA, Zekry A, Abouelatta M. LED Based Spectrophotometer can compete with conventional one. IJET. 2015; 4(2);399–407, https://doi.org/10.14419/ijet.v4i2.4504

23. Nandiyanto ABD, Zaen R, Oktiani R, Abdullah AG, Riza LS. A simple, rapid analysis, portable, low-cost, and Arduino-based spectrophotometer with white LED as a light source for analyzing solution concen- tration. TELKOMNIKA. 2018; 16(2):580–585, https://doi.org/10.12928/TELKOMNIKA.v16i2.7159

24. Verasa G, Silvaa EC, Lyraa WS, Soaresa SFC, Guerreiroa TB, Santos SRB. A portable, inexpensive and microcontrolled spectrophotometer based on white LED as light source and CD media as diffraction grid. Talanta. 2009; 77:1155–1159, https://doi.org/10.1016/j.talanta.2008.08.014 PMID: 19064105

25. Frisbie SH, Mitchell EJ, Sikora KR, Abualrub MS, Abosalem Y. Using polynomial regression to objec- tively test the fit of calibration curves in analytical chemistry. Int J Appl Mat Theor Phys. 2015; 1(2):14– 18, https://doi.org/10.11648/j.ijamtp.20150102.11

26. Frisbie SH, Mitchell EJ, Abualrub MS, Abosalem Y. Calculating the lowest reportable concentrations of toxic chemicals in the environment. Int J Appl Mat Theor Phys. 2015; 1(1):9–13, https://doi.org/10.11648/j.ijamtp.20150101.12

27. Davis S. Electronic design. Power: LDO voltage regulators. 2004. Available from: http://www.electronicdesign.com/power/power-ldo-voltage-regulators [accessed 31 August 2017].

28. Horowitz P, Hill W. The art of electronics. 3rd ed. New York, NY: Cambridge University Press; 2015. pp. 16, 202–207, 465, 829–834, 841–842.

29. Widenhorn R, Blouke MM, Weber A, Rest A, Bodegom E. Temperature dependence of dark current in a CCD. In: Blouke MM, Sampat N, Canosa J, Sampat N, editors. Proceedings of SPIE 4669, sensors and camera systems for scientific, industrial, and digital photography applications III. 2002; pp. 193–201, https://doi.org/10.1117/12.463446

30. Makarov SN, Ludwig R, Bitar SJ. Practical electrical engineering. Basel, Switzerland: Springer Interna- tional Publishing; 2016. p. 827.

31. Davis S. Schottky diodes: The old ones are good, the new ones are better. 2011. Available from: https://www.powerelectronics.com/discrete-power-semis/schottky-diodes-old-ones-are-good-new-ones-are-better [accessed 10 January 2019].

32. Hach Company. Spectrophotometers. 2018. Available from: https://www.hach.com/spectrophotometers/family?productCategoryId=35547203832 [accessed 22 June 2018].

33. Thermo Fisher Scientific. Spectronic™ 200 spectrophotometer. 2018. Available from: https://www.thermofisher.com/order/catalog/product/840-253500?ICID=search-product [accessed 22 June 2018].

34. United States Bureau of Labor Statistics. CPI inflation calculator. 2019. Available from: https://data.bls.gov/cgi-bin/cpicalc.pl [accessed 17 June 2019].

35. Agilent Technologies. Cary 60 UV-Vis. 2018. Available from: https://www.agilent.com/en/products/uv-vis-uv-vis-nir/uv-vis-uv-vis-nir-systems/cary-60-uv-vis [accessed 22 June 2018].

36. American Public Health Association, American Water Works Association, and Water Environment Federation. Rice EW, Baird RB, Eaton AD, Clesceri LS, editors. Standard methods for the examination of water and wastewater. 22nd ed. Washington, DC: American Public Health Association; 2012. pp. 1–6 to 1–36, 3–77 to 3–80, 4–77 to 4–88.

37. Hach Company. 1-(2-Pyridylazo)-2-naphthol PAN method. 2014. Available from: https://www.hach.com/asset-get.download.jsa?id=7639983728 [accessed 24 June 2017].

38. Harris DC. Quantitative Chemical Analysis. 5th ed. New York, NY: W.H. Freeman and Company; 1999. p. 103.

39. Skoog DA, West DM, Holler FJ, Crouch SR. Fundamentals of analytical chemistry. 9th ed. Belmont, CA: Brooks/Cole, Cengage Learning; 2014. pp. 658–674.

40. Christian GD. Analytical chemistry. 4th ed. New York, NY: John Wiley & Sons; 1986. pp. 371–377, 385.

41. United States Environmental Protection Agency. EPA drinking water method format. 2014. Available from: https://www.epa.gov/sites/production/files/2014-05/documents/ogwdw-methods-format.pdf [accessed 17 January 2019].

42. Dewitte K, Fierens C, Stöckl D, Thienpont LM. Application of the Bland–Altman plot for interpretation of method-comparison studies: A critical investigation of its practice. Clin Chem. 2002; 48(5):799−801, http://clinchem.aaccjnls.org/content/48/5/799 PMID: 11978620

43. Neter J, Wasserman W, Kutner MH. Applied linear statistical models. 2nd ed. Homewood, IL: Irwin; 1985. pp. 300–327.

44. World Health Organization (WHO). Guidelines for drinking-water quality. 4th ed. Geneva, Switzerland: WHO; 2011. pp. 472–475, https://www.who.int/water_sanitation_health/publications/2011/dwq_guidelines/en/

45. World Health Organization (WHO). Guidelines for drinking-water quality. Fourth edition incorporating the first addendum. 4th ed. Geneva, Switzerland: WHO; 2017. pp. 472–484, https://www.who.int/water_sanitation_health/publications/drinking-water-quality-guidelines-4-including-1st-addendum/en/

46. Snedecor GW, Cochran WG. Statistical methods. 7th ed. Ames, IA: The Iowa University Press; 1982. pp. 31–34.

47. International Union of Pure and Applied Chemistry. McNaught AD, Wilkinson A, editors. Compendium of chemical terminology. 2nd ed. Oxford, United Kingdom: Blackwell Scientific Publications; 1997. Nic M, Jirat J, Kosata B, Jenkins A, editors. XML on-line corrected version. 2014. Available from: http://goldbook.iupac.org/html/L/L03540.html [accessed 27 June 2017].

48. Gibbons RD, Coleman DE. Statistical methods for detection and quantification of environmental contamination. New York, NY: John Wiley & Sons; 2001. pp. 48–89.

49. United States Environmental Protection Agency. EPA method 200.8: Determination of trace elements in waters and wastes by inductively coupled plasma-mass spectrometry. 1994. Available from: https://www.epa.gov/sites/production/files/2015-06/documents/epa-200.8.pdf [accessed 15 January 2019].

50. Altman DG, Bland JM. Measurement in medicine: The analysis of method comparison studies. J R Stat Soc, Ser D Stat. 1983; 32(3):307–317, https://www.jstor.org/stable/2987937